JPL NO. 9950 – 602

(NASA-CR-168392) DESIGN STUDY OF IMAGING TECHNIQUES FOR THE STARPROBE MISSION Final Report (Ball Aerospace Systems Div., Boulder) 87 p HC A05/MF A01 CSCL 20F

N82-16849

Unclas
G3/74 08826

DESIGN STUDY OF IMAGING TECHNIQUES FOR THE STARPROBE MISSION

FINAL REPORT
F81-08
September 4, 1981

Ball Aerospace Systems Division
P.O. Box 1062, Boulder, Colorado 80306

Prepared for
Jet Propulsion Laboratory, California Institute of Technology
4800 Oak Grove Drive, Pasadena, California 91103
under Contract Number 955929

This work was performed for the Jet Propulsion Laboratory, California Institute of Technology sponsored by the National Aeronautics and Space Administration under Contract NAS7-100.

Prepared by:

Mark Bottema

M. Bottema,
Study Leader

Approved by:

D.A. Roalstad

D.A. Roalstad,
Study Manager

10 87

ABSTRACT

A 10-cm aperture, off-axis aplanatic gregorian telescope is investigated as a candidate instrument for imaging from Starprobe in the 115nm-900nm wavelength range. Focal lengths of 300cm (f/30) and 150cm (f/15) are compared in terms of optical performance, compatibility with the Starprobe spacecraft and response to the thermal environment in a 20-hour time interval, centered on perihelion. The general conclusion from this work is that UV/visible imaging from Starprobe should be technically feasible. A 10-cm aperture telescope with focal length close to 300cm is recommended for further study. This instrument should be capable of a detector-limited angular resolution of about 2 arc sec. The estimated overall dimensions should not exceed 105cm x 40cm x 25cm and its mass be less than 28kg. The recommended concept assumes solid-blank ULE mirrors, a graphite-epoxy optical bench and an aluminum thermal enclosure, covered with multi-layer insulation. These materials must be carefully selected to minimize the risk of UV photopolymerization of contaminants at the mirror surfaces during observations.

FOREWORD

This report is a draft of the Final Report of the Design Study of Imaging Techniques for the Starprobe Mission, performed by the Ball Aerospace Systems Division (BASD), for the Jet Propulsion Laboratory (JPL). The technical monitor at JPL was Dr. J.H. Underwood, Space Physics Section. At BASD, the study was done in the Space Systems Organization, under the cognizance of D.A. Roalstad, Manager of Advanced Programs for Science Instruments. The study participants and their responsibilities were:

Dr. M. Bottema, study leader	Optical design
M.E. Poyer	Mechanical design
Dr. D.E. Regenbrecht	Thermal design
R.P. Woolley, consultant	

SUMMARY

A concept for a visible-light/UV telescope (VUT) is developed in the following three stages:

1. Selection of candidate configurations for the VUT and an associated X-ray telescope (XRT).
2. Parametric analysis of an optical concept for an off-axis aplanatic gregorian telescope.
3. Development of a thermal control concept for the VUT.

Each of these stages is summarized below.

Candidate configurations. The scientific goals of the Starprobe mission require that the VUT and the XRT view the same region of the sun, i.e. their axes must be coaligned. Since the aperture of the XRT is an annulus, it is attractive to deflect the central part of the XRT beam to the VUT. This concept was developed in an earlier study (Ref. 1), but requires the XRT annulus to be larger than the VUT aperture and also makes it necessary to extract the VUT beam by one or more folding mirrors. Here an alternate configuration is presented, in which the VUT and XRT beams are completely separated. The thermally sensitive folding mirrors are then eliminated, as well as the constraints on the aperture diameters. This is a distinct advantage, since a parallel study of the XRT by American Science and Engineering (AS&E), Arlington, MA (Ref. 2) suggests that an annulus of the same diameter as the VUT aperture (10cm) would suffice to meet the Starprobe scientific requirements. With a reduced XRT aperture, the heatload from direct insolation into the two instruments need not necessarily be higher than with concentric beams. However, if a common heatshield baffle tube is maintained (Figure 1.1), its diameter must be larger.

Off-axis, aplanatic gregorian telescope. In a gregorian telescope, out-of-field radiation can effectively be eliminated by a heat-rejection mirror at the prime-focus fieldstop. In addition, excess radiation at the entrance

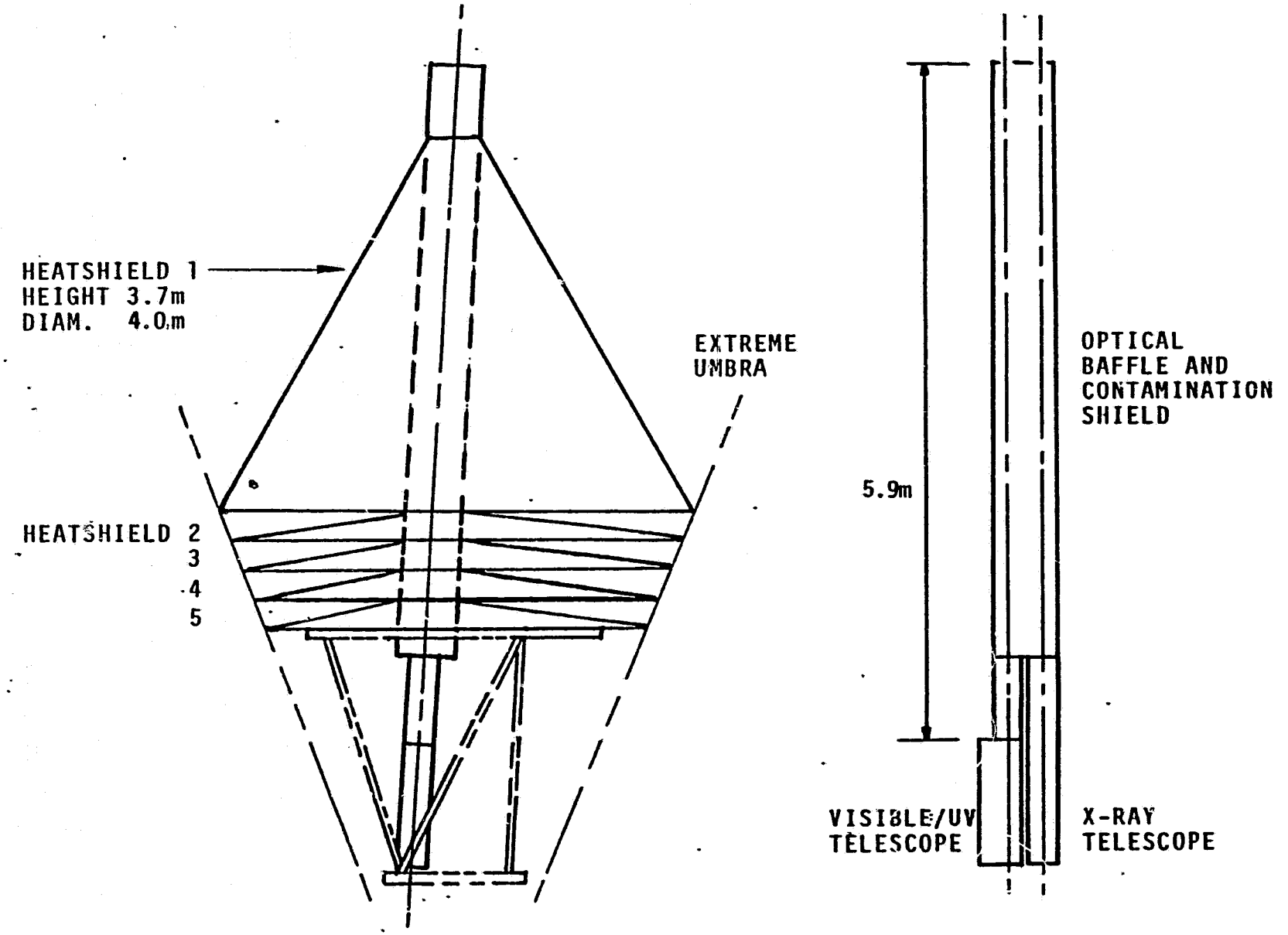

Figure 1-1 Imaging-instrument configuration

pupil can effectively be intercepted by a stop at the exit pupil. An off-axis entrance pupil offers an unobscured beam and does not degrade the image quality in an aplanatic telescope. This study assumes an aperture of 10cm diameter and a 12mm x 12mm CCD as the detector. Two focal lengths are compared, i.e. f = 300cm and f = 150cm. The angles, subtended by one detector pixel (15μm) are 1 arc sec and 2 arc sec, respectively. The corresponding fields of view are 0.23° x 0.23° and 0.46° x 0.46°. The latter is comparable in area to the sun as seen from the earth. The performance characteristics of the telescope depend primarily on the value, selected for the ratio of the telescope focal length to the primary mirror focal length. This ratio is equal to the secondary magnification m. A low value offers small residual aberrations and low susceptibility to thermally induced focus and alignment errors, but requires a large instrument. The reverse is true for a high value of m. In large earth-based telescopes, the entrance pupil is commonly placed at the primary mirror, in order to minimize its size. In the VUT it is advantageous to place the pupil either at the primary heatshield, in order to minimize the insolation, or at the aperture in the instrument enclosure, to minimize the heatloads from heat-shield radiation. Various parameter combinations are derived and compared. The instrument concept is shown in Figure 1-2.

Thermal control concept. The heatloads on the VUT stem from direct insolation within the VUT field of view, reradiation from the baffle tube and/or the heatshields and some parasitical heatleaks through the multi-layer insulation around the instrument. The VUT is cooled by radiation to space. The equilibrium temperature and thermal gradients within the instrument as a function of time from perihelion are calculated by computer modeling. The model is based on 40 nodes, which include a 3.7-m long primary heatshield and up to four secondary heatshields. The analysis assumes the VUT and XRT to be enclosed by a common thermal shroud. The instrument temperature is stabilized by means of thermostatic louvers, which are partially open at a distance of 10 solar radii and fully open at 4 solar radii. The temperature of the primary mirror can thus be kept constant at about 300K (27°C).

On the basis of the above analyses, a preliminary strawman VUT concept is identified. In general, the heatloads are smaller in the telescope with the

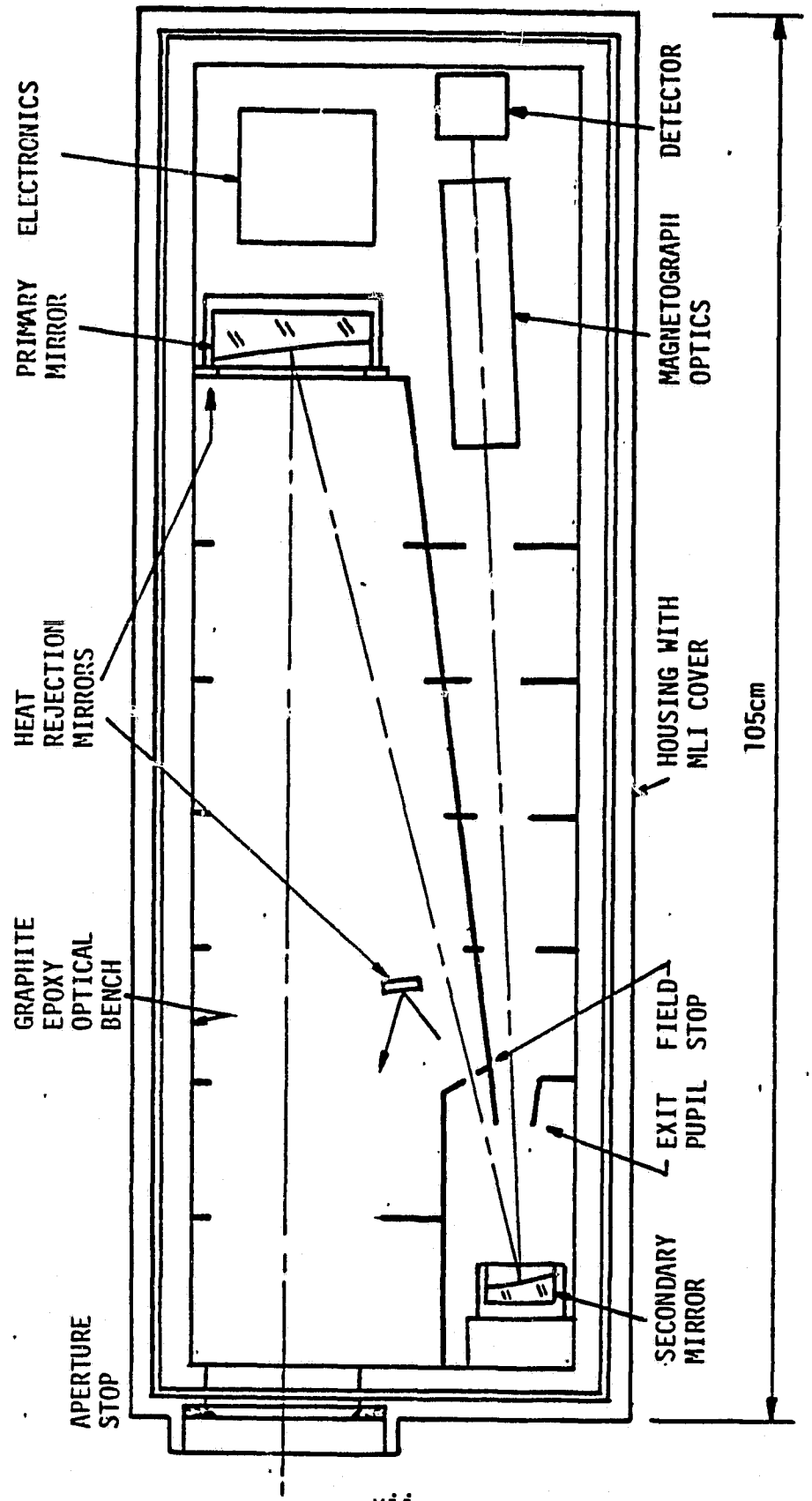

Figure 1-2 VUT instrument concept. The overall dimensions (without radiator) are 105cm x 40cm x 25cm.

smaller angular field, i.e. the larger focal length (f=300cm). This focal length also assures a detector-limited resolution of 2 arc seconds, based on the criterion that each resolution element should contain at least 2 detector pixels. Whereas alignment stability calls for a low secondary magnification, size and weight restrictions dictate a lower limit of m ≈ 5.5. An off-axis, aplanatic gregorian telescope with this magnification is recommended for further study.

TABLE OF CONTENTS

TABLE OF CONTENTS
(Continued)

TABLE OF CONTENTS
(Continued)

INTRODUCTION

The Starprobe mission is planned as part of NASA's long-term program for close-range observations of the sun. The scientific experiments, considered for this mission include (Ref. 1):

- Measurement of the solar quadrupole moment (J_2),
- Investigation of various field and particle phenomena near the sun,
- Imaging of the solar surface in the X-ray region and the visible-light/ultraviolet region.

The purpose of the present report is to evaluate the technical feasibility of instruments for the latter category, i.e. imaging in a wavelength range from approximately 115nm to 900nm. This range is of particular interest for the study of the dynamics of the photosphere and the evolution of solar magnetic fields. An instrument of very modest aperture (e.g. 10cm) suffices to reach a spatial resolution, better than that of the largest instruments, planned for earth orbit.

At the present time, the launch of Starprobe is planned for September, 1988. After a post-launch velocity change, the spacecraft swings by earth again in November, 1990; and then proceeds towards Jupiter. It will arrive there in March, 1992, and subsequently slow down to fall towards the sun. This is the so-called velocity change, Earth/Jupiter gravity-assist trajectory (ΔV-EJGA). Perihelion is expected to be reached in July, 1994. The planned perihelion distance is 4 solar radii from the sun's center. The spacecraft velocity is then over 300 km/sec. The trajectory passes over the solar poles. Polar transits occur at about ±6.7 hours from perihelion (Ref. 3).

The time interval of principal interest to imaging ranges from -10 hours to +10 hours from perihelion, with emphasis on the central 2 hours. The radiation environment is then extremely severe. At perihelion, the irradiance

at the spacecraft from solar thermal radiation alone is about 400 Wcm^{-2}. Expressed in the irradiance at earth (0.139 Wcm^{-2}) this amounts to 2888 "suns". At ±10 hours the spacecraft distance is about 10 solar radii and the irradiance drops to 64 Wcm^{-2} (461 "suns").

To cope with the thermal environment, effective shielding of the payload is necessary. In the present spacecraft concept, the primary heatshield is a tungsten-sheet cone with a base diameter of 4m and a height of 3.7m (Figure 1-1). This is followed by two or more secondary heatshields. The imaging instruments (X-ray telescope, XRT, and visible-light/UV telescope, VUT) are placed side by side and view a small portion of the sun through a central baffle tube. The tube is slanted at an angle of 3° with the spacecraft axis. In combination with a pointing offset of 7°, any point on the sun within a 10° radius from the sub-satellite point is accessible. At perihelion, the apparent sun diameter is about 29°.

The heatload on the imaging instruments consists mainly of direct insolation and heat radiation from the baffle tube and/or the heatshields. If the field of view is kept smaller than 0.5°, the direct insolation is less than in equivalent instruments in earth orbit. The specific problem in Starprobe is, therefore, the heatload from the heatshield radiation.

In view of the above, this report is structured as follows: After a recapitulation of the study goals and the study approach (Section 1), we compare various possible XRT/VUT configurations with regard to scientific merit and engineering complexity, and select a few for further study (Section 2). In Section 3 we identify an off-axis, aplanatic gregorian telescope as a suitable basis for the VUT and discuss its optical performance and thermal sensitivity as a function of its design parameters. This is followed by the development of a thermal control concept and a prediction of the instrument operational temperatures (Section 4). On the basis of this analysis, we select a "strawman" VUT concept and discuss some of its engineering aspects, such as structure, materials and contamination control (Section 5). Finally, we summarize the general conclusions from the present work and offer some recommendations for further study (Section 6).

13

Section 1
STUDY OBJECTIVES

The general objective, as defined in the Statement of Work (SOW), was to perform a feasibility and conceptual instrument design study of imaging techniques that can be used for the Starprobe mission. The specific study tasks, identified in the SOW, included:

A. Thorough familiarization with the scientific objectives of the imaging instruments, their interaction with the spacecraft and earlier design concepts and technical problems associated with these concepts.
B. Evaluation of alternate instrument design concepts, compatible with the Starprobe environment and spacecraft restrictions.

In accordance with the above directives, we established the following study approach:

1. Compare various candidate instrument configurations for the three imaging experiments, specified in the SOW, i.e. a magnetograph/ doppler velocity detector, an X-ray telescope and an XUV telescope.
2. Compare various candidate instrument concepts for each of the above three experiments in terms of their compatibility with Starprobe.

A contractually required "Informal Studyplan", detailing this approach, was submitted on May 1, 1981 (Appendix A). Since then, a separate study of X-ray imaging techniques was undertaken by AS&E. Consequently, we discontinued our design efforts of the XRT, and concentrated on imaging-instrument configurations (Section 2), optical design of the VUT (Section 3), and thermal control concepts for imaging-instrument package (Section 4). With regard to the latter, we initially assumed a spacecraft with a 7-m high primary heatshield, the baseline concept when the study was started (Ref. 1), but included also a 3.7m high primary heatshield, when the necessity of a reduction of height became apparent (Ref. 4).

19

Section 2
IMAGING-INSTRUMENT CONFIGURATIONS

2.1 CANDIDATE CONFIGURATIONS

A wide variety of conceivable arrangements for the XRT and the VUT is shown in Figure 2.1. Not included is a possible additional extreme-ultraviolet (XUV) telescope. A third instrument was not considered in this study.

The configurations in Figure 2.1 are arranged as follows: In configurations A through F the VUT and XRT are coaligned and have the same field of view. Among these, simultaneous observations are possible in A through D, but timesharing is necessary in E and F. In configuration G, the XRT and VUT share a small aperture in the primary heatshield (HS1) but have different fields. Finally, H and J represent the situation in which mission constraints would allow only one of the two instruments to be on board.

In configurations A, B, and C, the VUT beam is nested within the XRT beam. If a minimum VUT aperture diameter of 10cm is assumed, the inner diameter of the XRT annular aperture cannot be much smaller than 12cm, in order to allow for beam divergences and baffling.

Configuration A is the arrangement assumed in earlier studies (Ref. 1). Two diagonal mirrors are needed to extract the VUT beam. These mirrors may be exposed to temperatures as high as 650 K. Thermal deformations directly affect the image quality in the VUT. To minimize these deformations, uncoated sapphire flats have been proposed (Ref. 5). These introduce strong polarization, which may interfere with high-precision magnetograph experiments. Conceivably, the second mirror could be turned 90° to compensate the polarization from the first mirror. However, the VUT would then be closer to the secondary heatshields and also closer to the radio-isotope thermoelectric power generators (RTG), which may make shielding more difficult.

15

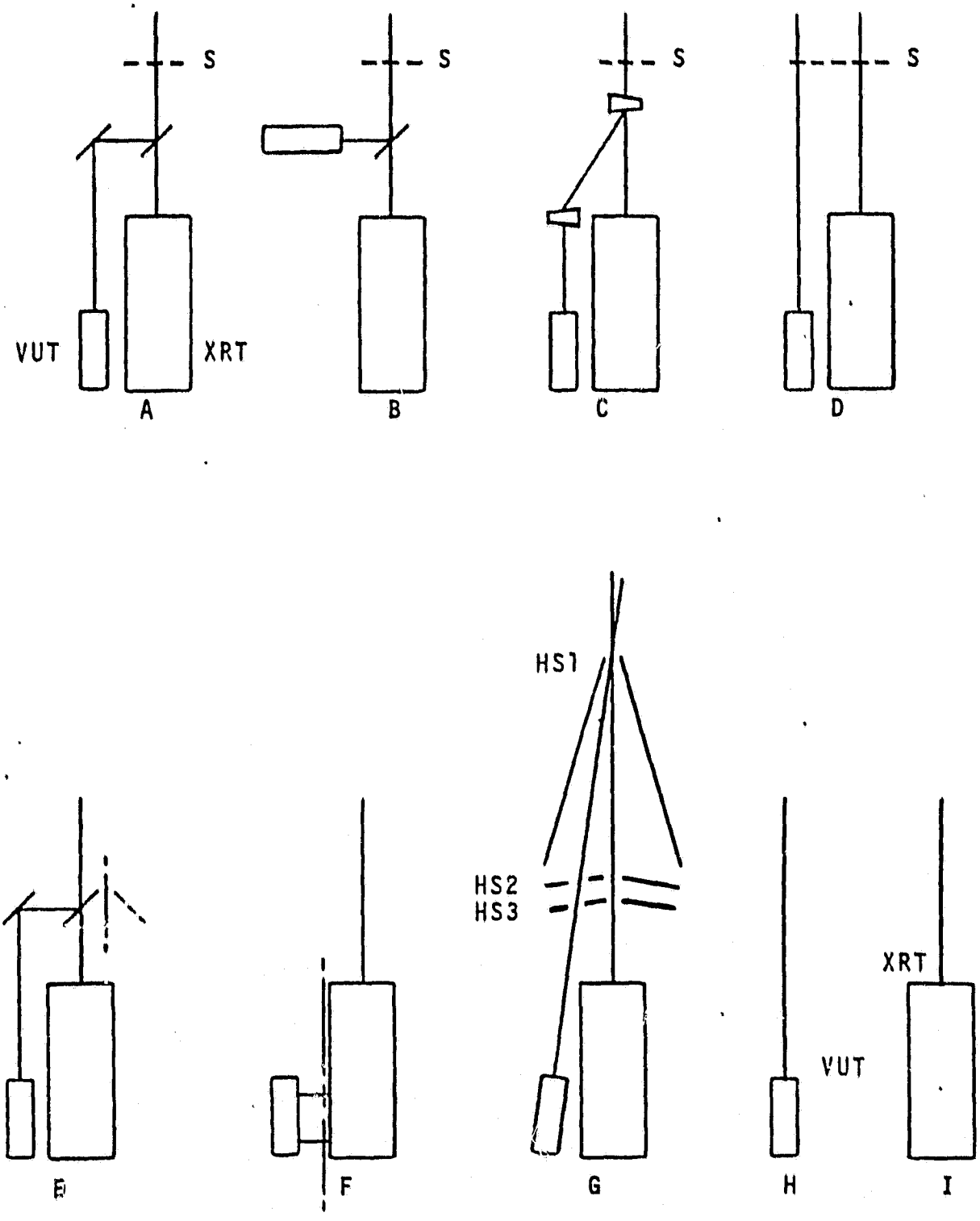

Figure 2.1 Candidate imaging-instrument arrangements. Configurations A, D, and H are selected for further evaluation.

In configuration B the second folding mirror is removed to eliminate its contributions to wavefront deformation. This is of little avail, however, since this contribution is expected to be small compared to that of the first folding mirror. In addition, the VUT location is subject to the same objections as above.

In configuration C, the folding mirrors are replaced by prisms. The wavefront deviations, caused by geometrical deformations are smaller, but deviations, caused by thermal changes in the refractive index are added. Since the two prisms may not come to the same equilibrium temperature, even first-order compensation may not be certain.

In configuration D the relay optics are eliminated and the XRT and VUT paths are completely separated. This has the distinct advantage that the XRT aperture can be chosen independently of the VUT aperture. In the four-mirror XRT concept, developed for Starprobe by AS&E, the outer and inner diameters of the aperture are 8.4cm and 9.6cm, respectively (Ref. 2). This, indeed, rules out a co-axial VUT light path. A disadvantage of configuration D is that two apertures are needed in the primary heatshield (HS1), with a corresponding increase in the heatload of the central baffle tube. However, as will be shown below, the heat input into the instruments need not at all be larger.

In configuration E a beam-steering mechanism is needed to direct the beam to the VUT. However, the reduction of the aperture diameter in HS1 does not warrant the additional mechanical complexity. Furthermore, the moveable folding mirror is subjected to a variable thermal environment, which may induce even larger deformations than in the static case. Timesharing might be acceptable for scientific observations, provided the instrument exchange is fast compared to changes in solar phenomena.

The mechanical complexity is even larger in configuration F, which requires rotation of a platform, carrying both instruments. However, no folding optics are needed.

17

Configuration G offers a small HS1 aperture and requires neither folding optics nor an exchange mechanism. However, the lack of coalignment between the XRT and the VUT is scientifically highly undesirable, if not totally unacceptable.

Obviously, none of the above problems are encountered if the VUT is the only imaging instrument (configuration H).

As shown symbolically in Figure 2.1, a shutter (S) might be placed near the VUT entrance. This may aid thermal control at perihelion and help equalize thermal conditions during the 20-hour interval of encounter. The shutter is not intended for precise exposure control, only as a thermal-control device (Section 4).

After consultation with JPL, it was decided to consider only configurations A, B, and H (with and without shutter) for further study. These are compared in detail below.

2.2 . COMPARISON OF SELECTED CONFIGURATIONS

The main difference between configurations A and D is the absence of VUT folding mirrors in the latter. Another difference lies in the size and number of the apertures, needed at the top of the primary heatshield (HS1), to admit sunlight to the instruments. An overview is presented in Figure 2.2. A single aperture (henceforth called HS1 aperture) suffices in configurations A and H, but two are needed in configuration D. Also indicated are the approximate sizes of the baffle tube that connects the HS1 aperture to the instruments.

Qualitatively, the main differences that can be inferred from Figure 2.2 are:

Heatloads on XRT and VUT. If the XRT and VUT have the same angular field of view, as is scientifically desirable, the HS1 aperture diameter in configuration A is defined exclusively by the XRT. Also, this aperture must be

18

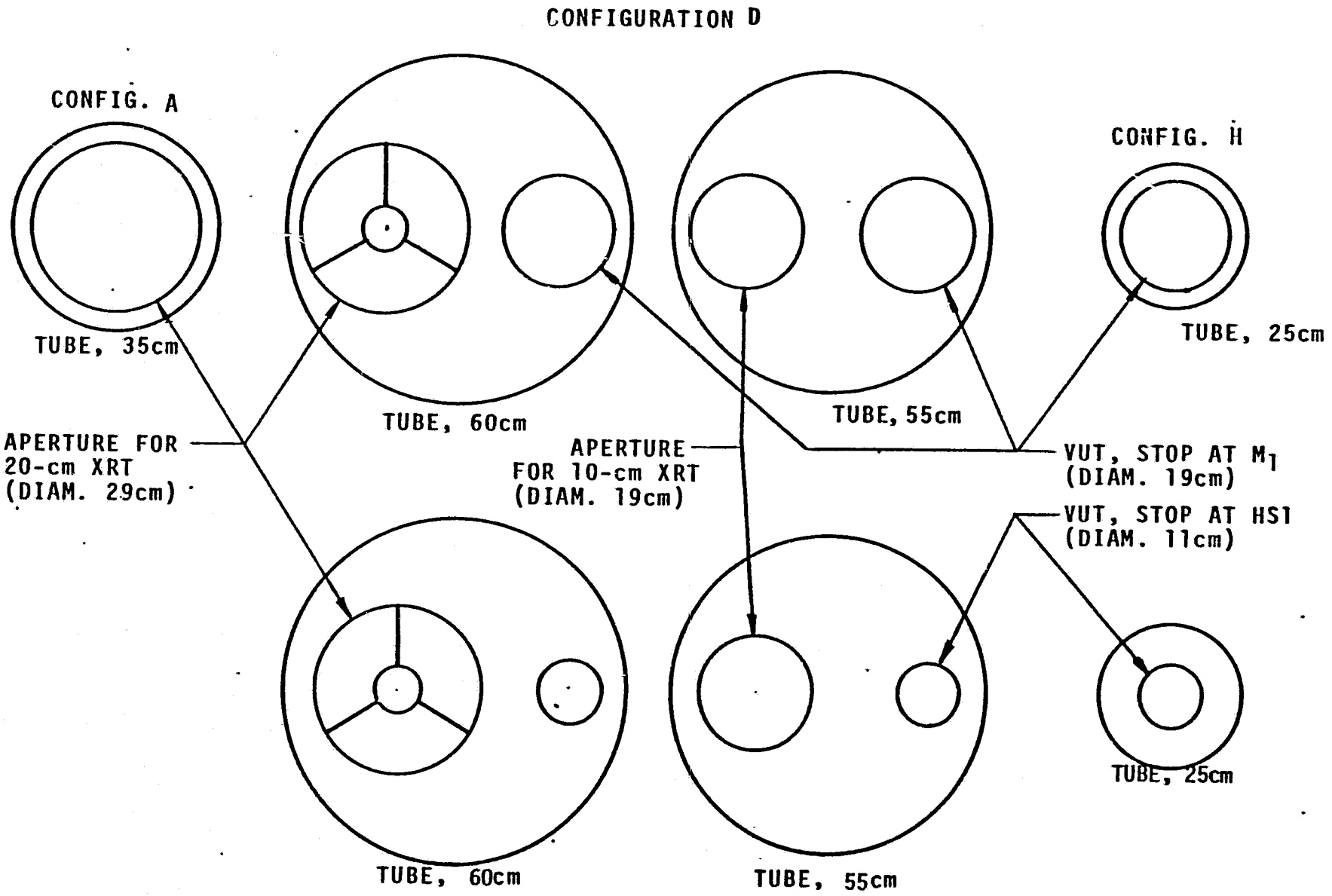

Figure 2.2 HS1 aperture and baffle tube diameters in three imaging-instrument configurations

unobscured to accomodate the VUT beam. The heatloads on the imaging instruments, caused by solar radiation, entering the HSI aperture (henceforth called "solar heatloads") are directly proportional to the area of this aperture. In configurations D and H, the HSI aperture sizes can be adjusted to closely match the individual beam diameters. As a result, the HSI aperture for the VUT (and, consequently, the solar heatload) is always smaller than in configuration A. However, in the latter case, the heatload is intercepted primarily by the folding mirrors and only a small portion reaches the actual instrument. With regard to the XRT, the heatload is either the same or smaller than in configuration A, depending on whether a central baffle in the HSI aperture is indeed technically feasible. This question will not be addressed in detail here.

Baffle Tube. Clearly, a larger diameter is required in configuration D than in configuration A. A narrower tube suffices if the VUT is the only instrument. In order to prevent solar radiation from reaching the instruments by internal reflections, the tube must be wider than the instrument beam and properly spaced internal baffle rings must be installed. In configuration D, these also serve to isolate the XRT and VUT beams from each other. Alternatively, separate tubes could be used for the two instruments. The choice involves the design of the entire heat-shield system and is not addressed in detail in this report. However, a single tube would seem more amenable to the accomodation of a third imaging instrument (e.g. XUV telescope), if considered for later addition. Undoubtedly, the solar heatload on the tube from the two apertures in configuration D is larger than in configuration A. However, this heatload appears to be negligibly small compared to the radiation, received from the primary heatshield and is, therefore, of little concern. Furthermore, the solar heatload could be readily reduced by a factor of 4 or 5 if an external baffle were placed in front of the HSI aperture, as shown in Figure 2.3. Most of the radiation, intercepted by this baffle, is diverted outside the primary heatshield. Whether such a baffle can indeed be accomodated and made resistant to the local thermal environment is primarily a matter of spacecraft design and is here not investigated further.

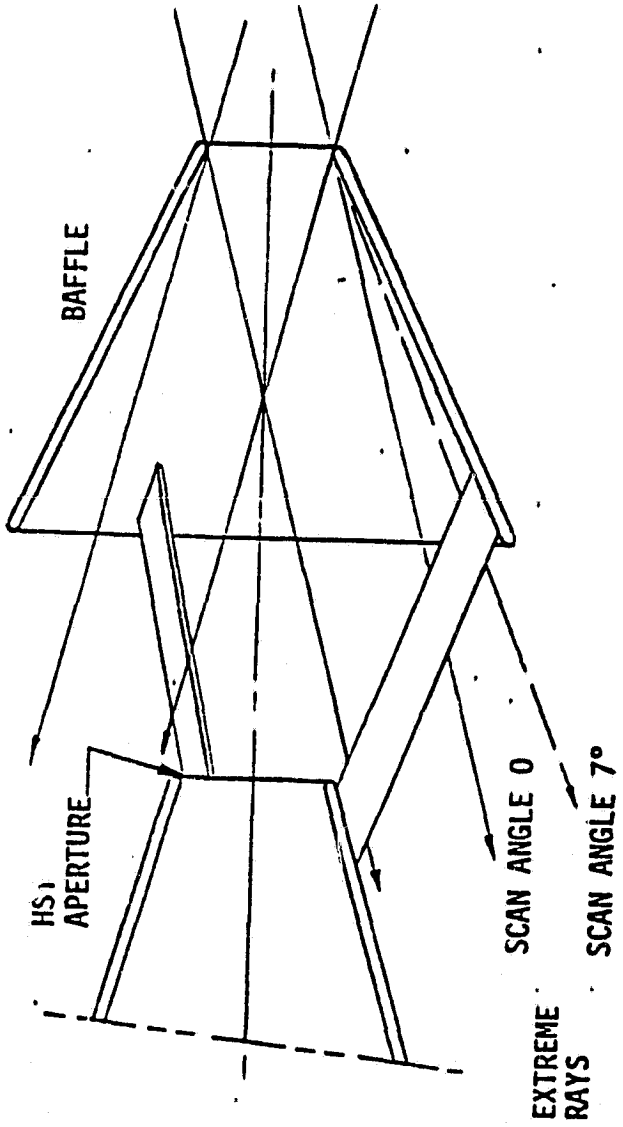

Figure 2.3 Heat rejection baffle in front of HSI aperture. The heatload at the aperture is reduced by narrowing the view angle.

2.3 HS1 APERTURES SIZES AND VUT SOLAR HEATLOADS

To substantiate the above comparisons, the HS1 apertures sizes for the XRT and VUT are derived quantitatively. In the case of the VUT, an estimate is made also of the associated solar heatloads.

2.3.1 HS1 Apertures for XRT

Examples of the HS1 apertures, needed for the XRT, are given in Table 2.1. Following the AS&E study report (Ref. 2), we assume a focal length of 3 m and a detector area of 12mm x 12mm. Although the actual field is square, we assume here a circular field, in order to simplify the calculations. The diameter of this field is equal to the diagonal of the detector. The corresponding angular diameter is 5.66 mrad = 0.324°. Three different aperture sizes are listed, i.e. O.D. = 20cm (derived from Ref. 1), O.D. = 12cm (minimum acceptable for configuration A), and O.D. = 8.4cm (derived from Ref. 2). In each case we assume the width of the annulus to be 1/8 of the outer diameter. We list two heatshield lengths, (7.0 m and 3.7 m) and assume the corresponding distances of the XRT primary mirror to the HS1 aperture to be 8.3 m and 5.0 m, respectively. The latter distance is estimated from Figure 1.1. To allow for thermal deformation of the spacecraft and the XRT mounting structure, the HS1 aperture diameter is arbitrarily made 1 cm larger than required for the XRT beam.

Obviously, the HS1 aperture must be larger for the higher heatshield and the larger XRT aperture. With a 3.7 m heatshield, the unobscured HS1 aperture, needed in configuration A for the smallest acceptable XRT diameter (12 cm) has an area of 197 cm^2, for instance. The area of the corresponding obscured area in configuration D is 162 cm^2. By comparison, the XRT, recommended in the AS&E study, requires an unobscured area of 142 cm^2. In this case, the reduction gained from a central baffle is only 16 cm^2. This may not warrant the technical complications involved.

TABLE 2.1
HS1 APERTURES FOR XRT

- o focal length 3 m
- o field diameter 0.324°

Primary heatshield height (m)	Annulus O.D. (cm)	Annulus I.D. (cm)	HS1 aperture Distance (m)	HS1 aperture O.D. (cm)	HS1 aperture I.D. (cm)	Area (cm^2) Obsc.	Area (cm^2) Unobsc.
7	20	17.5	8.3	25.7	11.8	409.1	518.6
	12	10.5	8.3	17.7	4.8	227.8	245.9
	9.6	8.4	8.3	15.3	2.7	178.0	183.7
3.7	20	17.5	5.0	23.8	13.7	299.1	445.9
	12	10.5	5.0	15.8	6.7	161.8	196.8
	9.6	8.4	5.0	13.4	4.6	125.2	141.6

2.3.2 HS1 Apertures for VUT

Examples of HS1 aperture sizes, needed for a 10-cm diameter VUT, are listed in Table 2.2. We consider two focal lengths, i.e. f = 300 cm and f = 150 cm. In each case we assume circular fields, with diameters 0.324° and 0.648°, respectively.

As will be shown in Section 3, the VUT entrance pupil can be placed at almost any distance from the primary mirror, without affecting the image quality. We list HS1 aperture diameters for three pupil locations, i.e. the primary mirror, the front aperture of the instrument enclosure and the HS1 aperture. The distances involved are derived from preliminary instrument concepts, similar to that in Figure 1.2, but with the instrument front aperture at 1.0 m from the primary mirror for f = 150cm and at 1.2 m for f = 300cm. Obviously, the HS1 aperture diameter increases with pupil distance and field angle, but is independent of these parameters if the entrance pupil is placed in the HS1 aperture.

2.3.3 VUT Solar Heatloads

The solar heatloads, associated with the HS1 aperture areas in Table 2.2, are listed in Table 2.3. The total flux, entering the instrument is calculated from the relation

D3

$$\phi_i = \pi^2 B r_i^2 r_a^2 / u_i^2, \qquad (1)$$

where B is the solar radiance at the center of the disk (B = 2490 $Wcm^{-2}sr^{-2}$, Ref. 6), r_i is the radius of the aperture in the instrument enclosure, r_a the radius of the HS1 aperture and u_i the distance between these apertures. In case the entrance pupil lies at the primary mirror or the HS1 aperture, r_i is taken to be 1 mm larger than the local beam radius.

TABLE 2.2
HS1 APERTURES FOR VUT

- o Entrance pupil diameter 10cm
- o Linear field diameter 17.0mm

Primary heatshield height (m)	Focal length (m)	Entrance pupil location	HS1 Aperture Distance (m)	HS1 Aperture Diameter (cm)	HS1 Aperture Area (cm^2)
7	3	Primary	9.8	16.5	215.0
		Instr. front	8.6	15.9	197.7
		HS1 aperture	0	11.0	95.0
7	1.5	Primary	9.8	22.1	383.2
		Instr. front	8.8	21.0	344.9
		HS1 aperture	0	11.0	95.0
3.7	3	Primary	6.5	14.7	169.2
		Instr. front	5.3	14.0	153.9
		HS1 aperture	0	11.0	95.0
3.7	1.5	Primary	6.5	18.4	264.6
		Instr. front	5.5	17.2	233.0
		HS1 aperture	0	11.0	95.0

Table 2.3 shows clearly that the flux into the instrument is smaller for the larger heat-shield height and the larger focal length (i.e. smaller angular field). For each combination, the flux is smallest when the entrance pupil is placed at the instrument front aperture, but only slightly smaller than when the pupil lies at the HS1 aperture. If neither the HS1 aperture or the instrument aperture were made oversize, the fluxes for pupil locations at the instrument

entrance and the HSl aperture would be the same, but still smaller than with the pupil at the primary mirror. For f = 3 m and heatshield height 3.7 m, these fluxes would be 87.3 W and 106.0 W, respectively.

TABLE 2.3
VUT SOLAR HEATLOADS

o HSl aperture areas from Table 2.2

Primary heatshield height (m)	Focal length (m)	Entrance pupil location	Heatloads			
			Instrument total flux Φ_i(W)	Primary mirror Total flux Φ_m(W)	Irradiance I_m (Wcm^{-2})	Suns
7	3	Primary	91.4	43.8	0.56	4.0
		Instr. front	67.3		0.51	3.7
		HSl aperture	71.5	48.0	0.25	1.8
7	1.5	Primary	124.2	78.0	0.99	7.2
		Inst. front	87.1		0.89	6.4
		HSl aperture	97.5	87.7	0.25	1.8
3.7	3	Primary	139.4	78.3	1.00	7.2
		Inst. front	111.5		0.91	6.5
		HSl aperture	115.2	84.7	0.56	4.0
3.7	1.5	Primary	219.6	122.5	1.56	11.2
		Inst. front	150.6		1.37	9.9
		HSl aperture	165.7	135.5	0.56	4.0

The value of B used in Table 2.3 applies to the center of the sun. Because of limb darkening, a smaller value applies for other pointing directions. The mean solar radiance is 2040 Wcm^{-2}sr^{-2} (Ref. 6). Other than that, Φ_i is independent of the distance of the Starprobe from the sun, as long as the angle, subtended by the sun is smaller than the field of view. For f = 3 m (4 mrad field) and f = 1.5 m (8 mrad field) these distances are 4.6AU and 2.3AU, respectively.

The incident flux Φ_m at the primary mirror is calculated similarly, i.e.

$$\Phi_m = \pi^2 B r_m^2 r_a^2 / u_m^2, \qquad (2)$$

25

where r_m is the radius of the exposed area of the mirror and u_m the distance to the HS1 aperture. When the entrance pupil lies at the HS1 aperture or at the instrument entrance, we assume r_m to be 1mm oversize. Without margins for alignment, the fluxes would be same with the pupil at the primary mirror and the HS1 aperture, but larger with the pupil at the instrument entrance. The values for f = 3 m and heatshield height 3.7 m would be 68.0 W and 87.3 W, respectively.

Also listed in Table 2.3 is the irradiance I_m at the center of the primary mirror. To compare this with instruments in earth orbit, I_m is expressed in "suns", i.e. the irradiance at earth (1 sun = 0.1388 Wcm^{-2}, Ref. 6). I_m is defined exclusively by the diameter of the HS1 aperture and its distance to the mirror, i.e.

$$I_m = \pi(r_a/u_m)^2 B. \qquad (2)$$

As will be shown in Section 3.2.2.2, the thermal deformation is, in first-order approximation, proportional to I_m. Evidently, this is smallest when the pupil lies at the HS1 aperture.

We note that all fluxes listed in Table 2.3 are only a very small fraction of the insolation at the HS1 aperture. At perihelion, the solar irradiance is about 400 Wcm^{-2}. Even for the smallest HS1 aperture (11cm diameter), the total incident flux is then 38kW.

2.3.4 Shutter

A shutter, placed at the instrument entrance, would block both the solar input and the heat radiation from the baffle tube and/or the secondary heatshields. However, the shutter itself may come to an equilibrium temperature, not much different from that of the baffle tube. Its effect would then be limited to the reduction of the solar heatload alone. Note that a duty cycle of 10%, for instance, would decrease the irradiation at the primary mirror to well below 1 sun in most cases. The thermal effects of a shutter are addressed in detail in Section 4.4.

2.4 CONCLUSIONS

a. An imaging-instrument configuration with separate light paths for the XRT and the VUT has three distinct advantages:

- o No image-degrading relay optics are needed to extract the VUT beam from the XRT beam.
- o Any combination of XRT and VUT aperture diameters can be accomodated, in particular an 8.4-cm XRT, recommended by a separate AS&E study, and a 10-cm VUT.
- o The solar heatloads into each instrument are smaller.

Two disadvantages are:

- o No attenuation of the solar heatload on the VUT by relay optics is available. However, the average heatload may be reduced by means of a shutter.
- o A wider baffle tube is needed and the solar heat input into this tube is larger. However, this input is negligibly small compared to that from reradiation of the heatshields.

b. The solar heatload on the VUT is smaller if the heat-shield height and the VUT focal length are larger. The total flux into the instrument is smallest if the entrance pupil is placed at the instrument front entrance but only little larger if the pupil lies at the HS1 aperture. The irradiance at the primary mirror is definitely smallest in the latter case.

27

Section 3
OPTICAL DESIGN CONCEPTS FOR VISIBLE-LIGHT/UV TELESCOPE

3.1 SCIENTIFIC OBJECTIVES AND PERFORMANCE GOALS

The main areas of scientific interest for imaging in visible and ultraviolet light from Starprobe are (Ref. 1):

- o Small-scale horizontal structures and velocity distributions in the photosphere.
- o Vertical structure of photosphere, derived from stereoscopic views.
- o Temporal changes in photosphere and globar solar oscillations.
- o Small-scale and global magnetic-field structures.

The structural details that can be resolved with earth-based telescope are usually not much smaller than about 200 km (0.3 arc sec) (Ref. 7). Only in moments of exceptionally good seeing might details of the order of 100 km be detected.

The proximity of Starprobe to the sun offers the opportunity to observe much finer details, even with a telescope of very small diameter. As pointed out by Zirin, the lower limit of structural sizes on the sun are not known (Ref. 8). Theoretical models of the photosphere suggest a pressure scale height of about 100 km and a photon mean free path of the same magnitude, but models of the transition region require sharp temperature differences over much smaller distances (Ref. 7). Zirin suggests a telescope of about 10cm aperture diameter. This would offer an angular resolution limit of about 1.5 arc sec, corresponding to 14 km at the subsatellite point at perihelion (Ref. 8). This diameter was accepted as a baseline in earlier Starprobe telescope concepts (Ref. 1).

The SOW for this study specifies an angular resolution of 2 arc sec. To derive the basic telescope parameters from this requirement, we assumed that the

detector to be used would be an 800 x 800 element CCD with a pixel size of 15μm x 15μm (area 12mm x 12mm). In order that this pixel size corresponds to an angle in object space of 10μrad (about 2 arc sec) a focal length f = 1.5m is required. However, to assure an angular resolution of 10μrad on the basis of the conventional criterion that each resolution element should have a width of at least 2 detector pixels, a focal length f = 3m is needed. To gain some insight of the effect of the focal length on various performance characteristics (e.g. size, image quality, thermal sensitivity) we decided to carry both values through most of the study.

The telescope field of view (FOV) is completely defined by the detector size, i.e.

f(m)	FOV
1.5	0.458° x 0.458° (0.648°, diagonal)
3.0	0.229° x 0.229° (0.324°, diagonal)

With regard to optical performance, we set as a design goal for this study that the telescope image quality shall be diffraction-limited at a wavelength λ_d of about 600 nm. This means that the actual telescope modulation transfer function (MTF) shall not fall below that of a perfect telescope at λ_d.

The achievable resolution in the recorded image depends not only on the telescope resolution but also on that of the detector. The combined resolution can readily be found by multiplication of the telescope MTF and the detector MTF. These can be derived as follows: for small field angles, the MTF of a perfect, unobscured telescope, as a function of the spatial frequency ν in the image plane, can be represented by

$$R_t(\nu) = (2/\pi)(\phi - \sin\phi\cos\phi), \qquad (1)$$

where R_t is the ratio of the modulation in the image to that in a sinusoidal pattern in the object. In Eq. (1)

$$\cos\phi = \nu/\nu_o, \qquad (2)$$

where ν_0 is the frequency at the resolution limit. This frequency is a function only of wavelength and f number, i.e.

$$\nu_0 = 1/(\lambda F\#). \tag{3}$$

The MTF of a CCD detector with pixel size s can be represented by the function

$$R_d(\nu) = \mathrm{sinc}(\pi\nu s). \tag{4}$$

The MTF of the telescope, combined with the detector, is simply the product of Eqs. (1) and (4).

By way of example, Figure 3.1 shows the MTF for an f/30 and an f/15 telescope at a wavelength of 666.7nm. This value was selected as an example to give round-number values for the limiting frequencies, i.e. $\nu_0 = 50$ cycles/mm (f/30) and $\nu_0 = 100$ cycles/mm (f/15). Also shown are the detector MTF for $s = 15\mu m$ and the product functions, $R(\nu) = R_t(\nu)R_d(\nu)$.

For low contrast objects, such as the photosphere structures, it is important to keep the modulation transfer ratio $R(\nu)$ reasonably high at the spatial frequencies of scientific interest. By way of example, the frequencies, for which $R(\nu) = 0.5$ and $R(\nu) = 0.25$ are listed in Table 3.1. Clearly, these are much smaller than the limiting frequency, which is defined either by the telescope (f/30) or by the detector (f/15). The spatial frequencies at the solar surface, corresponding to $R(\nu) = 0.5$ and $R(\nu) = 0.25$ depend on the ratio of the object distance and the focal length. Table 3.1 lists data for the subsatellite point at perihelion (distance 3 solar radii) and two focal lengths, i.e. f = 3 m and f = 1.5 m. Details, imaged with a contrast loss of a factor of four, are of the order of 25 km across for an f/30 telescope with f = 3 m and about 35 km across for an f/15 telescope with f = 1.5 m. In both cases the telescope aperture diameter is 10cm, which agrees with the value, recommended by Zirin. This aperture diameter is, therefore, accepted as a baseline for this study.

3°

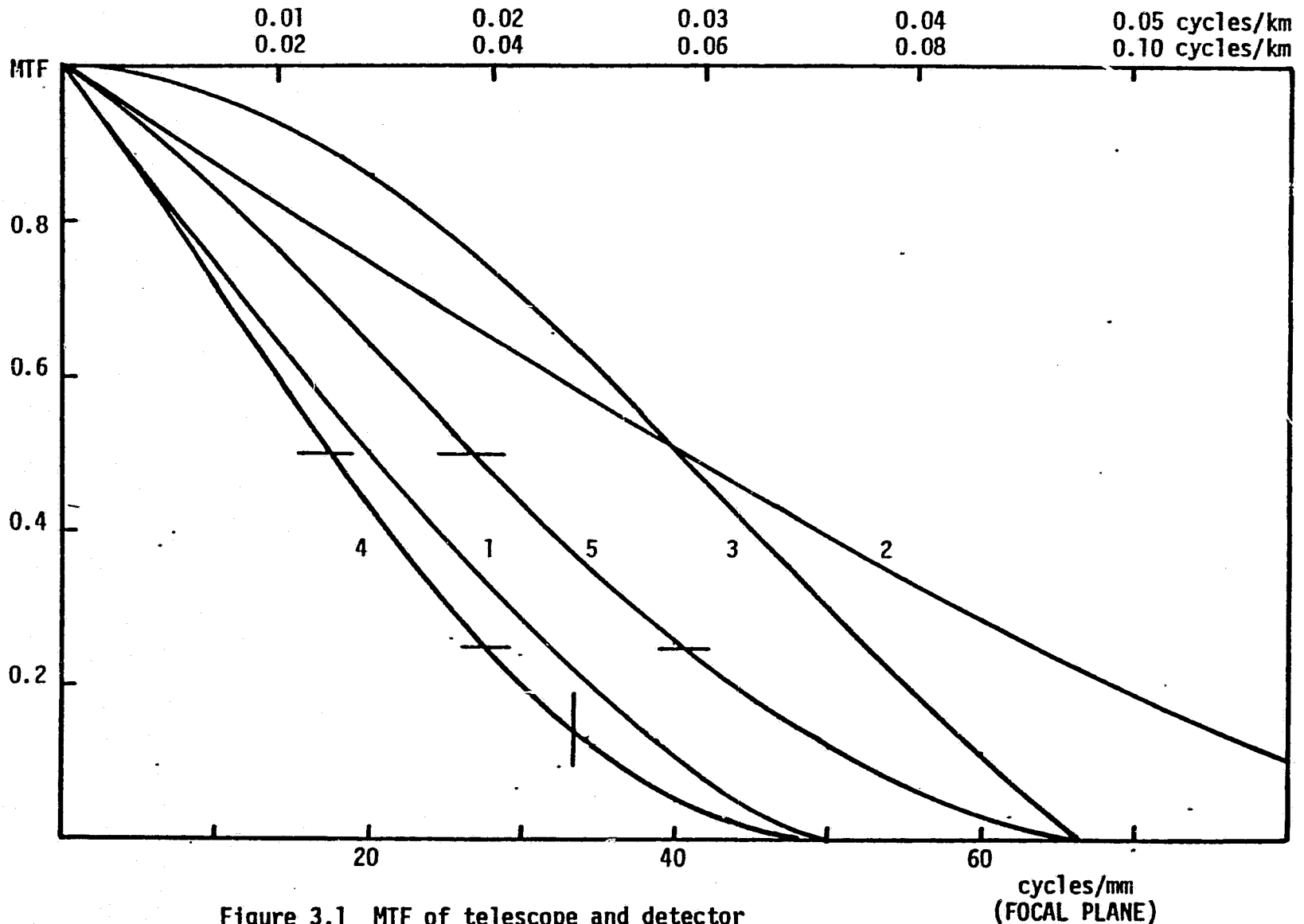

Figure 3.1 MTF of telescope and detector
Curve 1, f/30 telescope, λ = 667nm
Curve 2, f/15 telescope, λ = 667nm
Curve 3, CCD detector, 15μm pixels
Curve 4, product of (1) and (3)
Curve 5, product of (2) and (3)

TABLE 3.1

SPATIAL FREQUENCIES FOR MODULATION RATIOS 0.5 AND 0.25

- o λ = 666.7 nm
- o subsatellite point at 3 solar radii from surface

Focal length (m)	Diameter (cm)	F number	Spatial frequency: Image plane (mm^{-1}) R(ν)=0.5	Image plane (mm^{-1}) R(ν)=0.25	Solar surface (km^{-1}) R(ν)=0.5	Solar surface (km^{-1}) R(ν)=0.25
3	20	f/15	26.6	40.4	0.038	0.058
3	10	f/30	17.5	27.6	0.025	0.040
1.5	10	f/15	26.6	40.4	0.019	0.029
1.5	5	f/30	17.5	27.6	0.013	0.020

32

For a focal length of 3 m, the spatial frequency, corresponding to an angular resolution of 10μrad, is 33.3 cycles/mm. The modulation ratio in the f/30 telescope is then $R(\nu) \approx 0.14$. For f = 1.5 m, the corresponding frequency is 66.7 cycles/mm and, obviously, $R(\nu) = 0$.

The VUT wavelength range is assumed to be 115nm to 900nm. The lower limit is set by the reflectivity of Al/MgF_2 coated telescope mirrors, the upper limit by the spectral response of the CCD.

Whereas the image quality at long wavelength is primarily limited by diffraction, environmentally induced mirror deformations and alignment errors define the image quality at short wavelengths. If the rms wavefront aberrations do not exceed $\lambda_d/15$, the MTF is roughly independent of wavelength, i.e. the resolutions, listed in Table 3.1 apply also to the UV. This criterion should be set as a design goal for the VUT. The same approach was taken, for instance, in the design of the Space Telescope.

3.2 OFF-AXIS, APLANATIC GREGORIAN TELESCOPE

3.2.1 Telescope Concept

For solar observations, a gregorian telescope has two distinct advantages over a cassegrainian telescope:

a. The prime focus is accessible as a place for a fieldstop. This rejects all out-of-field radiation and minimizes the irradiation of the secondary mirror.
b. The exit pupil is also accessible as a place for a stop. In case the entrance pupil lies at the primary mirror, this stop merely acts as a straylight-rejecting stop. However, it acts as the actual aperture stop if the entrance pupil is placed at the HSI aperture or the instrument front aperture.

It is possible to aspherize the telescope mirrors in such a manner that third-order spherical aberration and coma are eliminated. This is called an aplanatic

telescope. In a gregorian telescope, this requires both mirrors to be ellipsoids. The only remaining third-order aberrations are then field curvature, astigmatism and distortion.

In a conventional, centered telescope, the obscuration by the secondary mirror and its support spiders causes uneven heating of the primary mirror. degrades the image quality and becomes a source of straylight. All this is eliminated in an unobscured, off-axis telescope. This can be created by simply decentering the entrance aperture in an otherwise centered system. An example is shown in Figure 3.2.

In an aplanatic telescope, the only third-order aberration, affected by decentering is distortion. Third-order astigmatism and curvature remain the same. These are also independent of the axial position of the entrance pupil. To be sure, higher-order aberrations become more prominent if the aperture is decentered, but in the VUT these remain negligibly small, since both the field and the aperture ratio are relatively small.

Given the focal length f, the optical parameters are defined mainly by the focal length of the primary mirror, f_1. The ratio $m = -f_1/f$ is called the secondary magnification. It is equal to the ratio of the secondary image distance, q, and the secondary object distance, p (Figure 3.2). To a lesser extent, the parameters are influenced by the location of the telescope image plane, relative to the primary-mirror vertex. This location can be defined by the ratio $s = -q/d$, where d is the separation of the two mirrors.

Telescope parameters for various values of m are given in Table 3.2 for f = -3 m and in Table 3.3 for f = -1.5 m. Following conventional sign rules, we count f, f_1, m, d and p negative in a gregorian telescope but q and the secondary focal length, f_2, positive. In each case, parameters are listed for two values of s, i.e. s = 0.8 and s = 1.2. The former offers the smallest overall telescope length, but allows accomodation of small scientific instruments only. With large, interchangeable instruments it is necessary to choose s > 1. Some of the telescope performance characteristics are discussed below.

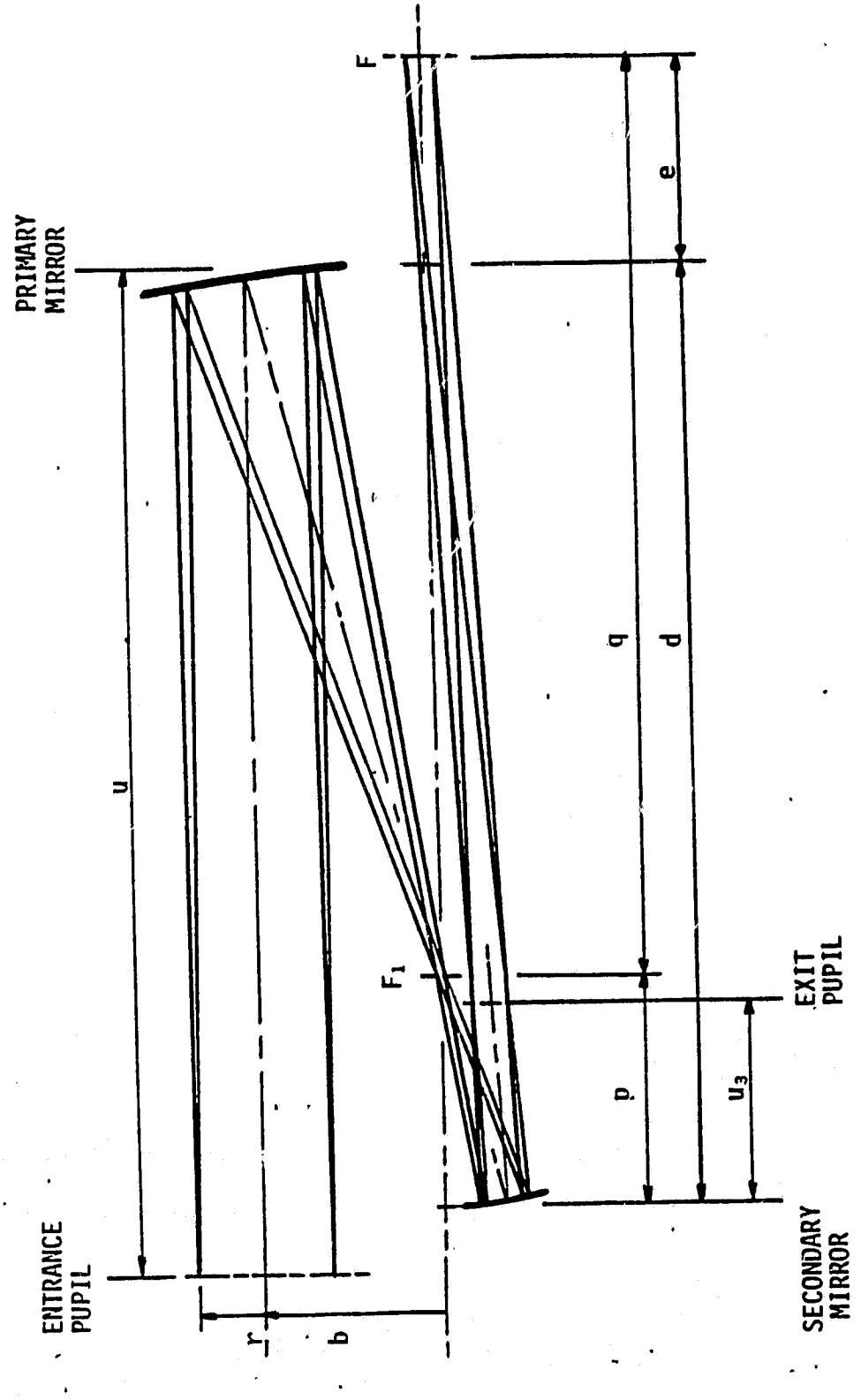

Figure 3.2 Gregorian telescope with decentered entrance pupil.

Table 3.2

TELESCOPE PARAMETERS

$f = -3m$, $r = 50mm$, $\alpha_o = 0.1625°$

m		-4		-5		-6		-8	
s		0.8	1.2	0.8	1.2	0.8	1.2	0.8	1.2
$-f_1$	(mm)	750	750	600	600	500	500	375	375
$-d$	(mm)	937.5	1071.4	714.3	789.5	576.9	625	416.7	441.2
f_2	(mm)	150	257.1	95.2	157.9	65.9	107.1	37.0	58.8
q	(mm)	750	1285.7	571.4	947.4	461.5	750	333.3	529.4
e	(mm)	-187.5	214.3	-142.9	157.9	-115.4	125	-83.3	88.2
A_3		2.313	1.375	2.938	1.792	3.563	2.208	4.8125	3.042
$-A_4$		9.688	6.458	15.313	10.208	22.188	14.792	39.688	26.458
$2\Delta y(\alpha_o)$	(μm)	0.2	0.4	1.4	1.2	3.2	2.4	8.2	5.7
$2\Delta x(\alpha_o)$	(μm)	3.9	2.6	6.1	4.1	8.9	5.9	15.9	10.6

Table 3.3

TELESCOPE PARAMETERS

$f = -1.5m$, $r = 50mm$, $\alpha_o = 0.325°$

m		-2		-3		-4		-5	
s		0.8	1.2	0.8	1.2	0.8	1.2	0.8	1.2
$-f_1$	(mm)	750	750	500	500	375	375	300	300
$-d$	(mm)	1250	1875	681.8	833.3	468.8	535.7	357.1	394.7
f_2	(mm)	333.3	750	136.4	250	75	128.6	47.6	78.9
q	(mm)	1000	2250	545.5	1000	375	642.9	285.7	473.7
e	(mm)	-250	375	-136.4	166.7	-93.8	107.1	-71.4	79.0
A_3		1.06	0.542	1.688	0.958	2.313	1.375	2.938	1.792
$-A_4$		2.19	1.458	5.313	3.542	9.688	6.458	15.313	10.208
$2\Delta y(\alpha_o)$	(μm)	3.3	1.1	2.3	0.5	0.7	1.5	5.7	4.9
$2\Delta x(\alpha_o)$	(μm)	3.5	2.3	8.5	5.7	15.5	10.3	24.5	16.3

3.2.2 Performance Characteristics

In preparation of the selection of the parameters m and s, most suitable for the VUT (Section 3.3), we present here a parametric analysis of the following characteristics:

- o Geometrical aberrations
- o Focus and alignment sensitivities
- o Entrance-pupil location and decentering
- o Heatloads on secondary mirror

As will be shown below, small aberrations and low focus/alignment sensitivity will require small absolute values of m. Quantative expressions in terms of m and s are derived. Some examples of the calculated image blur dimensions are given in Tables 3.2 and 3.3.

The heatload into the instrument depends on the axial location of the entrance pupil. This, in turn, drives the aperture-stop and exit-pupil locations, as well as the minimum decentering, required to assure an unvignetted field. Paraxial relations between these quantities are derived.

3.2.2.1 Geometrical Aberrations

In an astigmatic image, the rays come to a tangential line image in one curved plane (tangential image plane) and to a radial line image in a different plane (sagittal image plane). The radii of curvature of these planes are given by

$$r_t = \tfrac{1}{2}f/(2A_3+A_4) \qquad \text{(tangential image plane)} \qquad (5)$$

and

$$r_s = \tfrac{1}{2}f/A_4. \qquad \text{(sagittal image plane)} \qquad (6)$$

The aberration constants A_3 and A_4 are functions of m and s only. In an aplanatic telescope (Ref. 9)

$$A_3 = -\{2(m+s)-1\}/(4s) \quad (7)$$

and

$$A_4 = -(2m^2-1)/(4s). \quad (8)$$

The linear aberrations in the gaussian image plane are given by

$$\Delta y_0 = (2A_3+A_4)r\alpha^2, \qquad \text{(radial direction)} \quad (9)$$

$$\Delta x_0 = A_4 r\alpha^2, \qquad \text{(tangential direction)} \quad (10)$$

where r is the aperture radius and α the field angle. In general, Δx is larger than Δy in a gregorian telescope. In a flat image plane, the aberrations at the edge of the field (field angle α_0) can be balanced against those in the center by placing the image plane at a distance $(A_4/2)f\alpha_0^2$ from the gaussian focus, as indicated in Figure 3.3. The residual aberrations are then

$$\Delta y = 2A_3 r\alpha^2 + A_4 r(\alpha^2-\alpha_0^2/2), \quad (11)$$

$$\Delta x = A_4 r(\alpha^2-\alpha_0^2/2). \qquad \text{(best-matched flat image plane)} \quad (12)$$

The associated image blur diameters at full field are listed in Tables 3.2 and 3.3. The blur diameter on axis is equal to $2\Delta x(\alpha_0)$. The upper limit of $|m|$ has been selected to keep $2\Delta x$ smaller than about 1 pixel (15μm). In all of the above, distortion is considered to be of little consequence and is ignored.

3.2.2.2 Focus and Alignment Sensitivity

Of prime concern are uniform changes in temperature and axial thermal gradients in the mirrors. Their principal effect is a change in focus. Transverse gradients cause lateral image displacement and bending of the telescope. Each of these effects is discussed below.

38

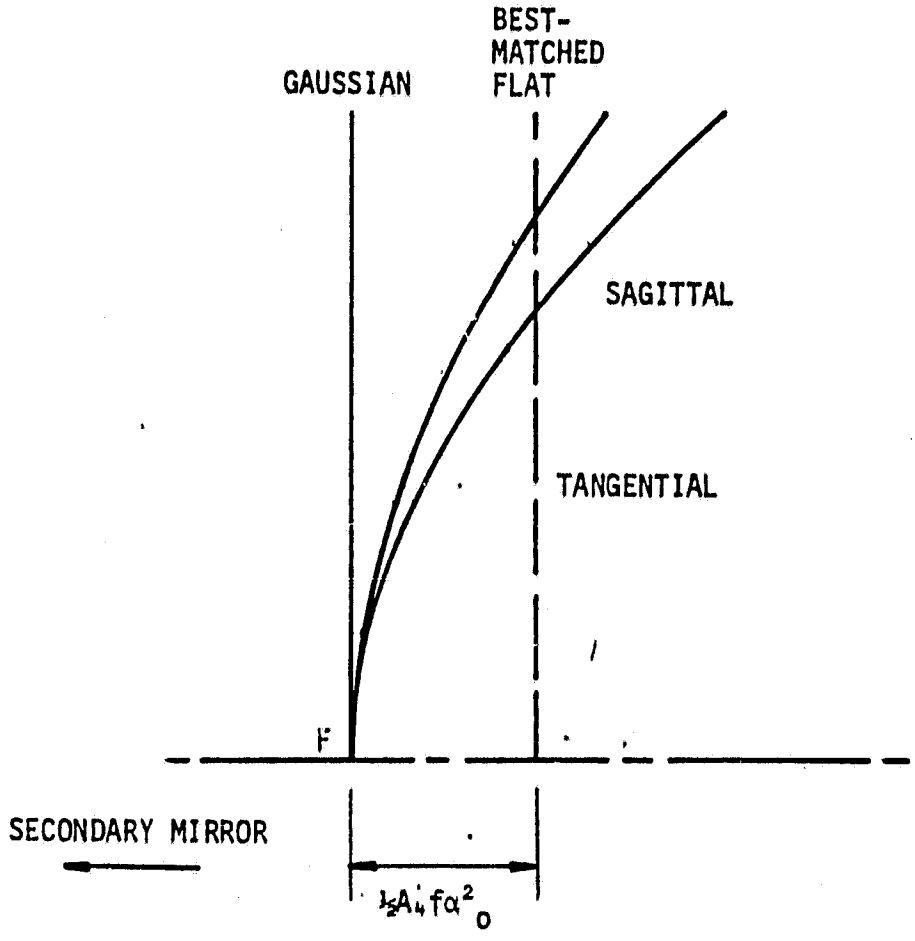

Figure 3.3 Image planes at gregorian focus

Isothermal focus changes. We assume that the two mirrors have the same coefficient of thermal expansion α_m and that all structural elements have the same coefficient α_s. The displacement Δf of the telescope image, relative to the detector, caused by a temperature change in each of the components, is then:

Primary mirror:

$$\Delta f_{prim} = -m^2 f_1 \alpha_m \Delta t_{prim} = m f \alpha_m \Delta t_{prim} \quad (13)$$

Mirror separation (assume primary mirror fixed):

$$\Delta f_d = (m^2+1) d \alpha_s \Delta t_d = -\{(m^2+1)/(m+s)\} f \alpha_s \Delta t_d \quad (14)$$

Secondary mirror:

$$\Delta f_{sec} = (m-1)^2 f_2 \alpha_m \Delta t_{sec} = -\{s(m-1)/(m+s)\} f \alpha_m \Delta t_{sec} \quad (15)$$

Back-focal distance, e = q + d:

$$\Delta f_e = -e \alpha_s \Delta t_e = -\{(s-1)/(m+s)\} f \alpha_s \Delta t_e \quad (16)$$

As can be readily verified, the sum of focus changes is zero if $\alpha_m = \alpha_s$ and Δt is the same for all four parameters.

If ULE is chosen as the mirror material, it would seem possible to make Δf_{prim} and Δf_{sec} negligibly small. The coefficient of thermal expansion (CTE) varies with temperature and crosses zero at a temperature that depends on the composition of the material. As will be shown in Section 4.4, primary mirror temperatures near 300K (27°C) and secondary mirror temperatures near 313K (40°C) may be expected during observations. ULE is defined as a material with a CTE between $\pm 3 \times 10^{-8}$ K^{-1} at 20°C and $4.5 \times 10^{-8} \pm 3 \times 10^{-8}$ K^{-1} at 60°C. It would certainly seem possible to obtain for each mirror material with a CTE within $\pm 3 \times 10^{-8}$ K^{-1} at the operating temperature.

For the structure we assume a graphite-epoxy (GE) tubular truss. An optical bench for the High-Resolution Spectrograph for the Space Telescope (under construction at BASD) was recently completed by Hercules, Inc., Wilmington, Delaware. Its coefficient of expansion is zero within $\pm 2 \times 10^{-7}$ K^{-1} at 294 K

90

(21°C). This is fairly close to the temperature of the VUT structure, predicted in Section 4. Hence, it would certainly seem feasible to keep α_s within $\pm 5 \times 10^{-7}\ K^{-1}$.

Numerical examples, based on the above data, are given in Table 3.4 for f = -3 m and representative values of m and s. We assume an uncertainty in the predicted structure and mirror temperatures of ±20 K. If the VUT temperature is thermostatically controlled, as described in Section 4, this seems a generous margin. The table shows the combination of $\alpha_m = 10^{-7}\ K^{-1}$ with $\alpha_s = 5 \times 10^{-7}$ K as well as $\alpha_s = -5 \times 10^{-7}\ K^{-1}$. The first offers partial compensation of the mirror and structure contributions. The focus changes for $\alpha_s = 0$ would be intermediate. The associated image swells are roughly proportional to m, but do not vary significantly with s. With f = -1.5 m, the focus changes would be half as large, but the geometrical image swell would be the same. These results indicate that the image swell can certainly be held to less than a pixel diameter, but low magnifications and partial compensation by proper selection of the CTE ranges are highly desirable.

Deformation of primary mirror. The response of the primary mirror to radiative heating of the front surface can be understood by the following elementary reasoning: The heatload ϕ_a, absorbed at the front surface, causes a temperature difference across the blank, equal to

$$\Delta T = t\Phi_a/(\pi\rho r_m^2), \tag{17}$$

where t is the blank thickness, r_m the radius and ρ the thermal conductivity. This temperature difference causes bending of the blank. In first approximation, the contribution to the curvature of the front surface is

$$\Delta c = \alpha\Delta T/t = \alpha\Phi_a/(\pi\rho r_m^2). \tag{18}$$

The associated primary focus change is

$$\Delta f_1 = -2f_1^2\Delta c = -2\alpha(f_1/r_m)^2\Phi_a/(\pi\rho). \tag{19}$$

91

Table 3.4

ISOTHERMAL FOCUS CHANGES

- o Structure $\alpha_s = \pm 5 \times 10^{-7}\ K^{-1}$
- o Mirrors $\alpha_m = 1 \times 10^{-7}\ K^{-1}$
- o Temp. Change $\Delta T = 20\ K$
- o Focal Length $f = -3\ m$

		Focus changes (μm)						Image swell (μm)	
m	s	Δf_{prim}	Δf_{sec}	Δf_d (α_s pos)	Δf_e (α_s pos)	Δf (α_s pos)	Δf (α_s neg)	(α_s pos)	(α_s neg)
2	0.8	12	12	-125	5	-96	144	3.2	4.8
2	1.2	12	27	-188	-8	-157	235	5.2	7.8
3	0.8	18	9	-136	3	-106	160	3.5	5.3
3	1.2	18	16	-167	-3	-136	204	4.5	6.8
4	0.8	24	8	-159	2	-125	189	4.2	6.3
4	1.2	24	13	-182	-2	-147	221	4.9	7.4
6	0.8	36	6	-213	1	-170	254	5.7	8.5
6	1.2	36	11	-231	-1	-185	279	6.2	9.3
8	0.8	48	6	-271	1	-216	324	7.2	10.8
8	1.2	48	10	-287	-1	-230	346	7.7	11.5

The corresponding telescope focus change is

$$\Delta f = -m^2 \Delta f_1 = 2\alpha(f/r_m)^2 \Phi_a/(\pi p). \qquad (20)$$

To estimate the contribution from solar heating, we assume that Φ_a is about 10% of the incident flux Φ_m (Table 2.3). With a 3.7 m heatshield, Φ_a is then about 8W. For ULE, $\rho = 0.013$ Wcm^{-1} K^{-1}. If we assume $\alpha = 3 \times 10^{-8}$ K^{-1}, we find the following changes and image swells:

Entrance-pupil location	r_m (cm)	Δf(μm)		Image swell (μm)	
		f = -3 m	f = -1.5 m	f = -3 m	f = -1.5 m
Primary	5.0	423	106	14.1	7.1
HST aperture	6.85	225	56	7.5	3.7

Conceivably, the focus could be set before flight to compensate for the expected focus change. This would allow a wider margin for uncertainties in the environmental conditions.

The above results show that it should be feasible to achieve adequate focus stability, without recourse to an active focus-control system. However, the mirror material must be very carefully selected (or perhaps specifically prepared) to assure sufficient low expansion at the operating temperature. Also, detailed modeling by computer of the mirror deformations will be necessary, taking into account the variation of the CTE with temperature. Such a model was constructed for a study of possible astronomical applications of the Shuttle Optical Telescope (SOT) (Ref. 10). It confirmed the approximate validity of Eqs. (17) and (19) and also showed that the figure errors, associated with bending of the blank, remain negligibly small if the focus change is controlled well.

Telescope bending. The first-order effect is a lateral displacement of the image. This will be negligibly small compared to spacecraft motion. If active image-motion compensation (IMC) is applied, it is fully eliminated.

Telescope bending also introduces third-order coma by tilt and decentering of the secondary mirror relative to the primary mirror. The aberration is the same in all field points. If no IMC is applied, the sagittal blur sizes associated with a tilt angle ε (center of rotation at secondary vertex) and a decenter distance Δ, are, respectively,

$$\Delta y_t = -(3/4)\{s(m^2-1)/(m+s)\}(r^2/f)\varepsilon \qquad (21)$$

and

$$\Delta y_d = -(3/4)(m^3+s)(r/f)^2\Delta. \qquad \text{(no IMC)} \quad (22)$$

With active IMC, decentering is compensated by tilt and Δy_d reduces to

$$\Delta y_d = -(3/8)\{(m+1)^2(m-1) + m + s\}(r/f)^2\Delta. \qquad \text{(IMC)} \quad (23)$$

Some examples of the blur sizes are given below. We assume ε = 1 mrad, Δ = 0.1mm and s = 1.

Blur Size (μm)	f = -3 m		f = -1.5 m	
	m = -3	m = -5	m = -3	m = -5
Δy_t	-2.50	-3.75	-5.00	-7.50
Δy_d (no IMC)	0.60	2.63	2.30	10.5
Δy_d (IMC)	0.15	0.96	0.58	3.83

Since coma is highly detrimental to image quality, the tolerance for Δy should not be set higher than about 1.5μm. However, when low-expansion materials are used for both the mirrors and the structure, the actual deformations will undoubtedly be much smaller than the above values for ε and Δ. Active alignment control will, therefore, certainly not be needed.

3.2.2.3 Entrance Pupil Location and Decentering

As pointed out in Section 2, the VUT entrance pupil may be placed at other locations than the primary mirror, in order to minimize heat inputs into the instrument. If the distance to the primary-mirror vertex is u, we can characterize the entrance-pupil location by the parameter

$$\mu = -u/f. \tag{24}$$

The primary mirror forms an image of the entrance pupil at a distance

$$u_1 = \mu f/(1+m\mu). \tag{25}$$

The distance of this intermediate image from the secondary vertex is

$$u_2 = (1-\mu s)f/\{(m+s)(1+m\mu)\}. \tag{26}$$

The final image, formed by the secondary mirror, is the exit pupil. Its distance from the secondary vertex is

$$u_3 = -s(1-\mu s)f/\{(m+s)(m+s-1+\mu s)\}. \tag{27}$$

If u is very large (as is the case when the entrance pupil lies at the HS1 aperture), the intermediate image lies close to the prime focus and becomes a suitable place for an aperture stop, as shown in Figure 3.4. The telescope output beam must clear this stop. This places a lower limit on the entrance-stop decentering distance, b_0. By straight-forward geometry it can be shown that this limit, as a function of r, α_0 and μ is given by

$$b_0 = [1 - 2(m+s)/\{(m+1)(1-\mu s)\}]r$$

$$+ [1 - \mu s - 2(m+s)/(m+1)](\alpha f/s). \qquad (\mu s>1) \tag{28}$$

As u decreases, the intermediate image approaches the secondary mirror and b_0 increases. As can be seen from Eq. (26), the intermediate image coincides with the secondary mirror if $\mu = 1/s$. Eq. (28) is no longer applicable (indeed the coefficient of r would become infinite) and must be replaced by the condition that the prime-focus fieldstop be cleared, i.e.

$$b_0 = r - 2f\alpha(m+s)/\{s(m+1)\}. \qquad (\mu s=1) \tag{29}$$

If $u < -f/s$, the intermediate image is not accessible and the aperture stop must be placed at the exit pupil. Under the condition that the exit pupil lies

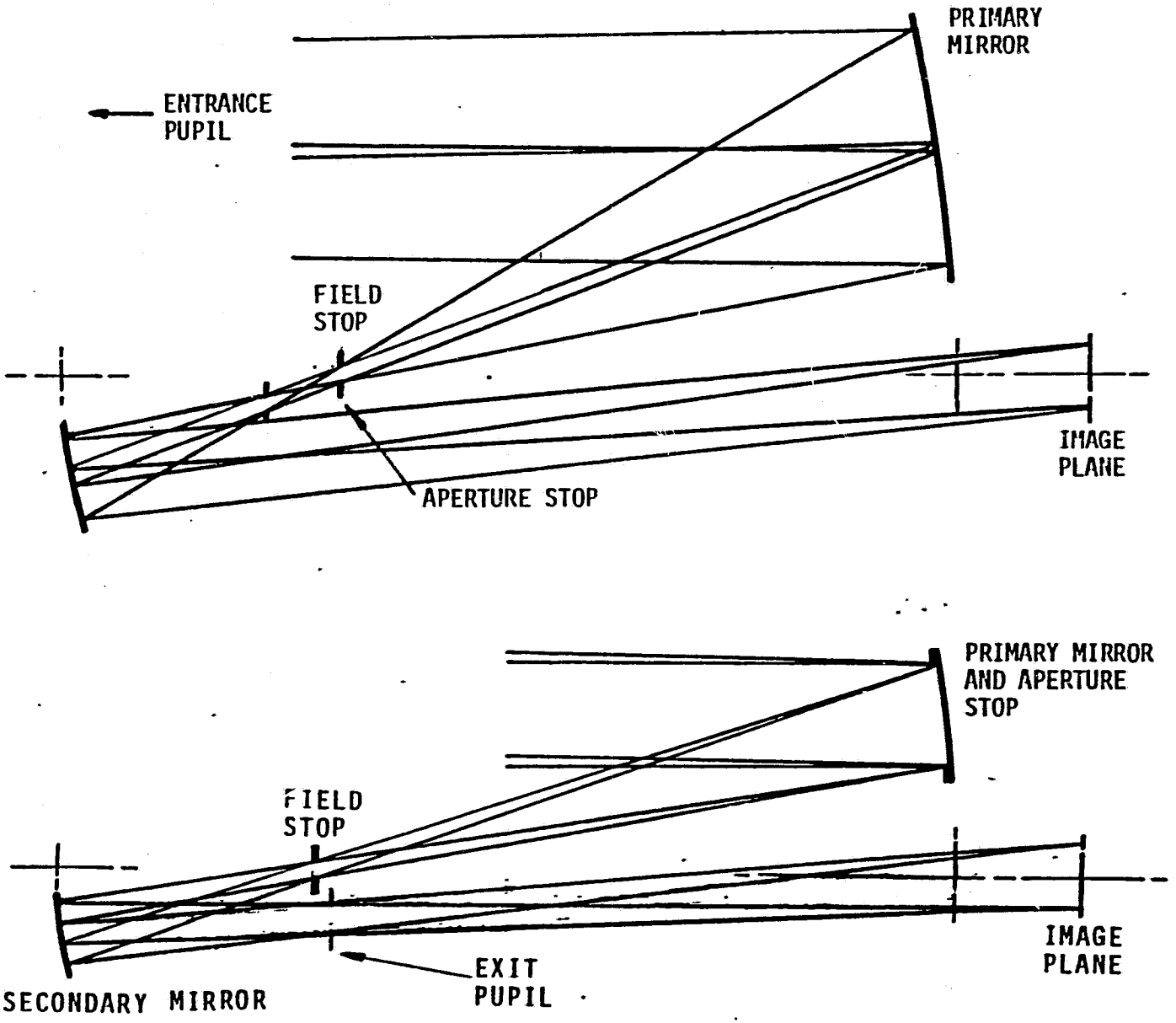

Figure 3.4 Telescopes with distant entrance pupil (top) and entrance pupil at primary mirror (bottom). Note difference in aperture stop location, mirror diameter and decenter distance.

between the secondary mirror and the prime focus, the minimum required distance is

$$b_o = [-1 + 2(m+s)/\{(m+1)(1-\mu s)\}]r$$

$$+ [1 - \mu s - 2(m+s)/(m+1)](\alpha f/s). \qquad (\mu s<1) \quad (30)$$

In case the entrance pupil lies at the primary mirror, Eq. (30) reduces to

$$b_o = \{(m+2s-1)/(m+1)\}(r - \alpha f/s). \qquad (s<1,\ \mu=0) \quad (31)$$

This equation applies only if $s < 1$. If the exit pupil lies between the prime focus and the primary mirror ($s>1$), the decenter distance is defined by the condition that the beam, reflected by the secondary mirror, clears the prime-focus fieldstop (Figure 3.4). This requires

$$b_o = r - \alpha f/s. \qquad (s>1,\ \mu=0) \quad (32)$$

Examples of the minimum required distances are given in Tables 3.5 and 3.6. These are definitely smallest when the pupil lies at the primary mirror. If the pupil is moved towards the instrument front, u_3 decreases and b_o becomes larger. This can be inferred from the data, obtained in case the entrance pupil would lie in the plane of the secondary mirror. Even more decentering is needed when the pupil lies at the HSI aperture (the exception is pupil at instrument front and low magnification with f = -1.5 m). However, none of the distances listed seem impractically large, even though the actual decentering must be considerably larger than b_o in order to allow for the physical structure of the stops.

We note that the exit pupil lies in inifinity when

$$\mu = -(m-1+s)/s. \qquad \text{(telecentric telescope)} \quad (33)$$

The beam divergence is then fully symmetrical in all field points. This may be of interest with regard to polarizers, etalons and filters in the scientific instruments.

Table 3.5

MINIMUM ENTRANCE-PUPIL DECENTERING DISTANCE

$f = -3m$, $r = 50mm$, $\alpha = 0.1625°$

m	s	Decenter distance, b_0(mm)			
		Entrance pupil at primary mirror	Entrance pupil in plane of secondary mirror	Entrance pupil at HS1 aperture	
		$\mu = 0$	$\mu = -1/(m+s)$	$u = 9.8m$ (7-m HS1) $\mu = 3.27$	$u = 6.5m$ (3.7-m HS1) $\mu = 2.17$
-4	0.8	68.7	122.9	155.9	225.9
-4	1.2	57.1	130.6	115.9	132.9
-5	0.8	66.7	110.6	154.5	223.3
-5	1.2	57.1	107.2	116.7	134.2
-6	0.8	65.5	104.1	153.7	221.7
-6	1.2	57.1	96.9	117.2	134.9
-8	0.8	64.1	97.0	152.8	219.9
-8	1.2	57.1	87.6	117.7	135.8

Table 3.6

MINIMUM ENTRANCE-PUPIL DECENTERING DISTANCE

$f = -1.5m$, $r = 50mm$, $\alpha = 0.325°$

m	s	Decenter distance, b_0(mm)			
		Entrance pupil at primary mirror	Entrance pupil in plane of secondary mirror	Entrance pupil at HS1 aperture	
		$\mu = 0$	$\mu = -1/(m+s)$	$u = 9.8m$ (7-m HS1) $\mu = 3.27$	$u = 6.5m$ (3.7-m HS1) $\mu = 2.17$
-2	0.8	84.9	332.0	167.0	246.9
-2	1.2	57.1	224.9	123.1	116.5
-3	0.8	72.8	139.5	158.7	231.2
-3	1.2	57.1	230.4	121.1	124.2
-4	0.8	68.7	106.9	155.9	225.9
-4	1.2	57.1	122.5	120.4	126.8
-5	0.8	66.7	93.4	154.5	223.3
-5	1.2	57.1	97.5	120.1	128.0

98

3.2.2.4 Solar Heatloads

The heatloads at the instrument entrance and the primary mirror for different entrance-pupil locations are summarized in Section 2.3.3. Here we calculate the corresponding heatloads at the prime-focus fieldstop and the secondary mirror.

Prime-focus Fieldstop. If R is the primary-mirror reflectivity, the total flux incident on the stop is

$$\phi_f = R\phi_m \tag{34}$$

The fraction transmitted by the stop depends somewhat on the aperture stop location. If the latter lies at the primary mirror, the transmitted flux is

$$\phi_t = \pi R r^2 \Omega B, \qquad \text{(aperture stop at primary)} \tag{35}$$

where r is the aperture stop radius and Ω the solid angle, subtended by the field. For a round stop, $\Omega = \pi\alpha^2_o$. For the inscribed square, matching the CCD detector, $\Omega = 2\alpha^2_o$. In case the entrance pupil lies at the HS1 aperture or the VUT front entrance, ϕ_t is larger. The upper limits are

$$\phi_t = \pi R r_a^2 \Omega B, \qquad \text{(entrance pupil at HS1)} \tag{36}$$

$$\phi_t = \pi R r_i^2 \Omega B. \qquad \text{(entrance pupil at instrument front)} \tag{37}$$

Numerical data are listed in Table 3.7. The incident flux depends on the distance of the HS1 aperture, but the transmitted flux does not.

Secondary Mirror. If the entrance pupil lies at the primary mirror, the incident flux is

$$\phi_s = \phi_t = \pi R r^2 \Omega B. \qquad \text{(entrance pupil at primary or HS1)} \tag{38}$$

If the pupil is placed at the HS1 aperture, the secondary mirror is preceeded by the aperture stop. The incident flux is then the same.

49

Table 3.7
SOLAR HEATLOAD AT PRIME-FOCUS FIELDSTOP

Heatshield height	7 m		3.7 m	
Focal length	3 m	1.5 m	3 m	1.5 m
Incident flux, ϕ_f (W)				
Pupil at primary	39.4	70.2	70.5	110.3
Pupil at HS1 apert.	43.2	78.9	76.2	122.0
Transmitted flux, ϕ_t (W)				
Pupil at primary	4.4	17.7	4.4	17.7
Pupil at HS1 apert.	5.4	21.4	5.4	21.4

Table 3.8
IRRADIANCE AT CENTER OF SECONDARY MIRROR

m	s	Irradiance, ϕ_s			
		f = -3 m		f = -1.5 m	
—	—	Wcm^{-2}	Suns	Wcm^{-2}	Suns
-2	0.8	--	--	0.51	3.7
-2	1.2	--	--	0.10	0.7
-3	0.8	0.43	3.1	1.70	12.3
-3	1.2	0.13	0.91	0.51	3.7
-4	0.8	0.90	6.5	3.60	26.0
-4	1.2	0.31	2.2	1.23	8.8
-5	0.8	1.55	11.2	6.21	44.7
-5	1.2	0.56	4.1	2.26	16.3
-6	0.8	2.38	17.1	9.52	68.6
-6	1.2	0.90	6.5	3.60	26.0

50

If the entrance pupil lies at the instrument front entrance, the aperture stop follows the secondary mirror and the flux is somewhat larger. The upper limit is

$$\phi_s = \pi R r_i^2 \Omega B. \qquad \text{(entrance pupil at instrument front)} \qquad (39)$$

Only the central area of the secondary mirror is illuminated evenly. In case the aperture stop lies at the primary mirror, the radius of this area is

$$r_{s,inner} = -sr/(m+s) - \alpha f/(m+s). \qquad (40)$$

The illumination tapers off to an outer radius

$$r_{s,outer} = -sr/(m+s) + \alpha f/(m+s). \qquad (41)$$

The irradiance in the central area is

$$I_s = R\{(m+s)/s\}^2 \Omega B. \qquad (42)$$

Numerical examples are given in Table 3.8. Evidently, I_s increases sharply with the secondary magnification m. It is also significantly larger when $s < 1$, because of the higher secondary-mirror power required.

In tables 3.7 and 3.8 we assume a mirror reflectivity R = 0.9. This is a representative value for MgF_2 coated Al in the visible and relevant to thermal radiation. The UV reflectivity decreases rapidly below 120nm and depends on the thickness of the MgF_2 coating. Reflectivities that can be achieved with a thickness of 25nm are listed below

λ(nm)	R
190	0.82
170	0.80
150	0.79
130	0.83
120	0.82
110	0.47
105	0.17

51

3.3 VUT PARAMETER SELECTION

3.3.1 Selection Criteria

The four parameters to be selected are the focal length, the secondary magnification m, the image distance/mirror separation ratio s, the entrance pupil location and its decenter distance b. The selection is based on the following criteria

- Geometrical aberrations,
- Thermal focus sensitivity,
- Heatloads on primary and secondary mirror,
- Instrument size.

Geometrical Aberrations. Astigmatism and defocusing both cause uniform widening of the image and are, therefore, very similar in their effects on image quality. The total-system MTF is not seriously degraded if the image blur diameter is smaller than 1 pixel. Somewhat arbitrarily, we assign 1/3 of this tolerance to astigmatism, in order to leave 2/3 to environmentally induced defocusing.

The maximum-permitted values of m, corresponding to $2\Delta x = 5\mu m$ are listed below, together with the image distance q and the mirror separation d, which characterize the instrument length for $s > 1$ and $s < 1$, respectively.

f (m)	-3	-3	-1.5	-1.5
s	0.8	1.2	0.8	1.2
m	-4.53	-5.53	-2.35	-2.74
q (mm)		842		1170
d (mm)	-804		-1045	

An interesting result of this comparison is that the instrument length is actually smaller for the larger focal length.

52

Isothermal Focal Change. As follows from Table 3.4, small magnifications are preferable, but no sharp selection criteria for m or s can be derived. The limitations on m, established above, are quite acceptable.

Deformation of Primary Mirror. The focus change is independent of m and s, but the geometrically calculated image swell is smaller for the shorter focal length. However, if the focus change in Eq. (20) is compared to the diffraction focal depth, $\Delta f = \frac{1}{2}(f/r)^2\lambda$, as would certainly be justified in the visible, the longer focal length offers the larger tolerance.

Heatload on Primary Mirror. As shown in Section 3.2.2.2, the solar irradiance is definitely smaller if the entrance pupil is placed at the HSI aperture. However, the heatload from reradiation from the heatshields is smaller when the entrance pupil is placed at the instrument front aperture. A detailed thermal stress analysis of the primary mirror and its environment would be needed to decide which location offers the least susceptibility to deformation. This is beyond the scope of the present study.

On the basis of the entrance-pupil decentering distances needed, the primary mirror is strongly preferred as the location for the entrance pupil (Tables 3.5 and 3.6). For f = 1.5 m, we recommend this location, although the heatloads on the primary mirror are about 10% higher (Table 2.3). For f = -3 m, we consider the difference in b_o too small to warrant this increase and recommend the instrument entrance as the pupil location.

Heatload on Secondary Mirror. The central solar irradiances for the secondary-magnification limits, established above, are the following:

f (m)	-3 m	-3 m	-1.5 m	-1.5 m
m	-4.53	-5.52	-2.34	-2.74
s	0.8	1.2	0.8	1.2
Irradiance (Wcm^{-1})	1.22	0.73	0.84	0.37
(suns)	8.8	5.3	6.1	2.7

On the basis of these numbers, we definitely recommend a telescope arrangement with s > 1. The irradiance is distinctly smaller if f = -1.5 m. However, it does not exceed the solar irradiance at the primary mirror, even if f = -3 m. The solar irradiance in this case is about 6.5 suns if the entrance aperture lies at the instrument entrance (Table 2.3).

Instrument Size. The instrument length is smaller for f = -3 m than for f = -1.5 m, if the geometrical aberrations in the field are the same. This favors the choice of the larger focal length. The length is larger for s > 1, but not by more than 5% to 10%. This disadvantage is completely overruled by larger space, available for scientific instruments, especially if several interchangeable instruments have to be accomodated.

The instrument height is defined primarily by the decenter distance and the primary-mirror diameter. In order to allow for the physical structure of the field and aperture stops, the actual decenter distance b should be about 30mm larger than the minimum distance b_o in Tables 3.5 and 3.6. In case f = -3 m, this amounts to about 135mm if the pupil lies at the instrument entrance, as compared to 90mm if the pupil lies at the primary mirror. This difference amounts to about 10% of the total estimated instrument height, and should be considered insignificant.

The instrument width is primarily defined by the primary mirror diameter and is virtually independent of other telescope parameters.

3.3.2 Preliminary VUT Parameters

In order to assure at least some modulation transfer at an angle of 2 arc sec, a focal length of at least 3 m is necessary (Section 3.1). Since no compelling reason was found in the preceeding sections to reduce the focal length, we accept this value for the preliminary VUT definition.

To keep the secondary-mirror irradiance low, we select s ≈ 1.2. A magnification m ≈ -5.5 is then needed to keep the geometrical image blur within 1/3 pixel.

Round-number parameter values, based on the above selections are listed in Table 3.9. These are used as a basis for the preliminary instrument definition in Section 5. The optical diagram is shown in Figure 3.2. The solar heatload into the instrument front entrance is 94.4 W*. The heatloads on the mirrors and the stops are given in Table 3.10. These are calculated by the methods, established in Sections 2.3.3 and 3.2.2.4, under the assumption that the physical diameters of the front aperture and the primary mirror are 10.2cm and 10.6cm, respectively. The primary mirror is illuminated uniformly only over a central area of 9.6cm diameter. At the edge, the irradiance drops to 74% of the central value, listed in Table 3.10.

It is of interest to compare the solar heatloads in VUT with those in a ground-based solar telescope, such as the California Institute of Technology photoheliograph at the Bear Lake Observatory. As is shown in Table 3.10, the incident flux at the primary mirror is much smaller than in the photoheliograph, but the irradiance is 6.4 times higher. We note that this number would be considerably lower if a 7-m primary heatshield were used (Table 2.3).

At the prime focus, the heat to be rejected is much smaller in the VUT than in the photoheliograph. The reason is that most heat rejection in Starprobe is done by the baffle system preceeding the primary mirror. Problems, encountered in the photoheliograph with deterioration of the prime-focus heat-rejection mirror are not likely to occur in the VUT.

The central irradiance at the secondary mirror in the VUT is higher by a factor of 1.7. However, experience with the photoheliograph should still be valuable to predict the environmental effects in the VUT.

---

*About 74% of this heatload is reflected back through the aperture by the heat-rejection system, leaving a net entering solar heatload of only 25 W (Table 4.4).

55

Table 3.9
PRELIMINARY VUT PARAMETERS
$m = -5.5$
$s = 11/9 \approx 1.22$
$\mu = 0.27$

Focal length		f (mm)	-3003
Aperture diameter		2r (mm)	100
F number		F#	30
Primary mirror			
focal length		f_1 (mm)	- 546
conic constant		C_1	- 0.98531
Mirror separation		d (mm)	- 702
Secondary mirror			
focal length		f_2 (mm)	132
conic constant		C_2	- 0.51044
object distance		p (mm)	- 156
image distance		q (mm)	858
Entrance pupil			
distance primary		u (mm)	810.81
decenter distance		b_o (mm)	135
Exit pupil			
distance secondary		u_3 (mm)	116.19
diameter		$2r_u$ (mm)	24.70
Field of view		$2\alpha_o$	0.324°
Field diameter			
prime focus		$-2f_1\alpha_o$ (mm)	3.09
gregorian focus		$-2f\alpha_o'$ (mm)	16.97
Curvature/astigmatism			
astigmatism constant		A_3	1.955
curvature constant		A_4	- 12.170
mean radius curvature		ρ_m (mm)	146.98
Best-matched flat field			
sagittal blur (α_o)		$2\Delta y$ (μm)	1.74
tangential blur ($0,\alpha_o$)		$2\Delta x$ (μm)	4.86

56

Table 3.10
VUT COMPARED WITH BEAR LAKE PHOTOHELIOGRAPH

		VUT	PHOTOHELIOGRAPH (Ref. 11)
BASIC PARAMETERS			
f	(mm)	-3003	-32500
u	(mm)	750	0
2r	(mm)	100	650
m		-5.5	-13
s		11/9	13/11
α	(mrad)	2.826	0.465
PRIMARY MIRROR			
f_1	(mm)	-546	-2500
Total incident flux	(W)	77.7	461
Absorbed	(W)	7.8	
Irrad. (center)	(Wcm^{-2})	0.89	0.14
	(Suns)	6.4	1
PRIME-FOCUS FIELDSTOP			
Total incident flux	(W)	69.9	387
Transmitted	(W)	4.6	13.5
Rejected	(W)	58.8	336
Absorbed	(W)	6.5	37
SECONDARY MIRROR			
Total incident flux	(W)	4.6	13.5
Irrad. (center)	(Wcm^{-2})	0.69	0.41
	(Suns)	5.0	3.0
APERTURE STOP			
Total incident flux	(W)	4.1	
Transmitted	(W)	4.0	

57

3.4 CONCLUSIONS

- An off-axis aplanatic gregorian telescope is identified as suitable for imaging from Starprobe in UV/visible light.
- The focal length is 3 m, the aperture 10cm. The angular resolution limit, defined by 10% modulation transfer, is smaller than 2 arc sec.
- The geometrical aberrations are smaller than 5μm (1/3 pixel) in a 17mm diameter field.
- The entrance aperture is placed at the instrument front aperture to minimize heatloading by radiation from the heatshields.
- With a 3.7-m primary heatshield, the solar irradiance is 6.5 suns at the primary mirror and 5.0 suns at the secondary mirror. These numbers would be smaller with a 7-m primary heatshield.
- An elementary estimate shows that adequate passive focus stability should be achievable by use of graphite-epoxy for structure and ULE for the mirrors. However, the composition of these materials must be selected to make the thermal coefficient of expansion very close to zero at the operating temperature.
- Detailed computer modeling of the primary mirror and its environment is necessary to verify the validity of the last conclusion.

4.0 THERMAL CONTROL OF IMAGING INSTRUMENTS

During the study, we examined the spacecraft-instrument system with its environment at 4 sun radii and 10 sun radii, developed a small (8 nodes) thermal analytical model (TAM) to serve as the interface for the instrument model, performed trade-offs and arrived at a baseline spacecraft configuration for the study, created a more detailed TAM (35 nodes) of the spacecraft/XRT/VUT, and performed trade-offs demonstrating that the thermal design concept is feasible. The simple TAMS permit many trade-off analyses to be performed quickly with minimum cost.

This section describes the baseline design concept, analyses, trade-offs, conclusions and recommendations resulting from the study.

4.1 OPERATIONAL REQUIREMENTS

The two imaging instruments are the Visible-light/Ultraviolet-light Telescope (VUT) and the X-ray Telescope (XRT). For a common view of the sun, it was considered practical to coalign them with a common mount. Therefore, for this study the VUT and XRT are considered in the same thermal package on the spacecraft. Each would have its own thermal control design, and the temperature requirements are similar.

This study is directed primarily toward the VUT. The spacecraft and XRT are included in only the detail necessary to demonstrate the effects of a representative environment.

The VUT is required to remain operational during the time the spacecraft is between 10 sun radii and 4 sun radii which corresponds to the period within ±10 hr of perihelion. The instruments must remain aligned and the electronics remain functional within specifications during this encounter portion of the mission. In addition, the subsystems must survive all aspects of the long flight prior to the encounter.

4.2 ENVIRONMENTAL INTERFACE ANALYSIS

In order to obtain a thermal environment for the VUT, a simplified TAM of the preliminary spacecraft heatshield system as shown in Reference 1 was constructed early in the study. This was updated to a shorter HSI cone, made of tungsten, to represent the concept as of July, 1981. The simplified interface TAM did not contain all of the equipment aft of the last heatshield--only the imaging instrument package, as shown in Figure 4-1. The TAM contained 7, 8, or 9 nodes depending on the inclusion of 3, 4 or 5 heatshields. Comparison of the results of this analysis agreed well with the preliminary results from the much more detailed JPL model and is, therefore, adequate to support this study.

Table 4-1 gives the thermal properties used in the Ball interface TAM. The emissivities were kept constant at the values for elevated temperature. Taking into account that the emissivity will be lower for the shields that are cooler would result in a cooler environment for the instrument package. Therefore, the analysis is "conservative" which is proper for this phase of the program development.

A trade-off was performed on the number of heatshields to include.. There is room for a maximum of five. The results are shown in Table 4-2 and demonstrates that the more the better. Therefore, it was agreed with JPL that we should use the five shield configuration in our instrument model.

Table 4-3 gives a summary of other trade-off considerations examined with the interface TAM.

4.3 VUT INSTRUMENT ANALYSIS

The nodes 6 and 9 were removed from the interface TAM and a more detailed instrument package was included in their place. The instrument package nodes are identified in Figure 4-2. This TAM contains 35 nodes and has sufficient detail to indicate temperature gradients in the VUT structure and the temperature of the critical components. The aperture model was reworked to more accurately account for the gradient in the baffle tube; and the direct solar energy absorbed by the mirrors, field stop and detector package was properly distributed.

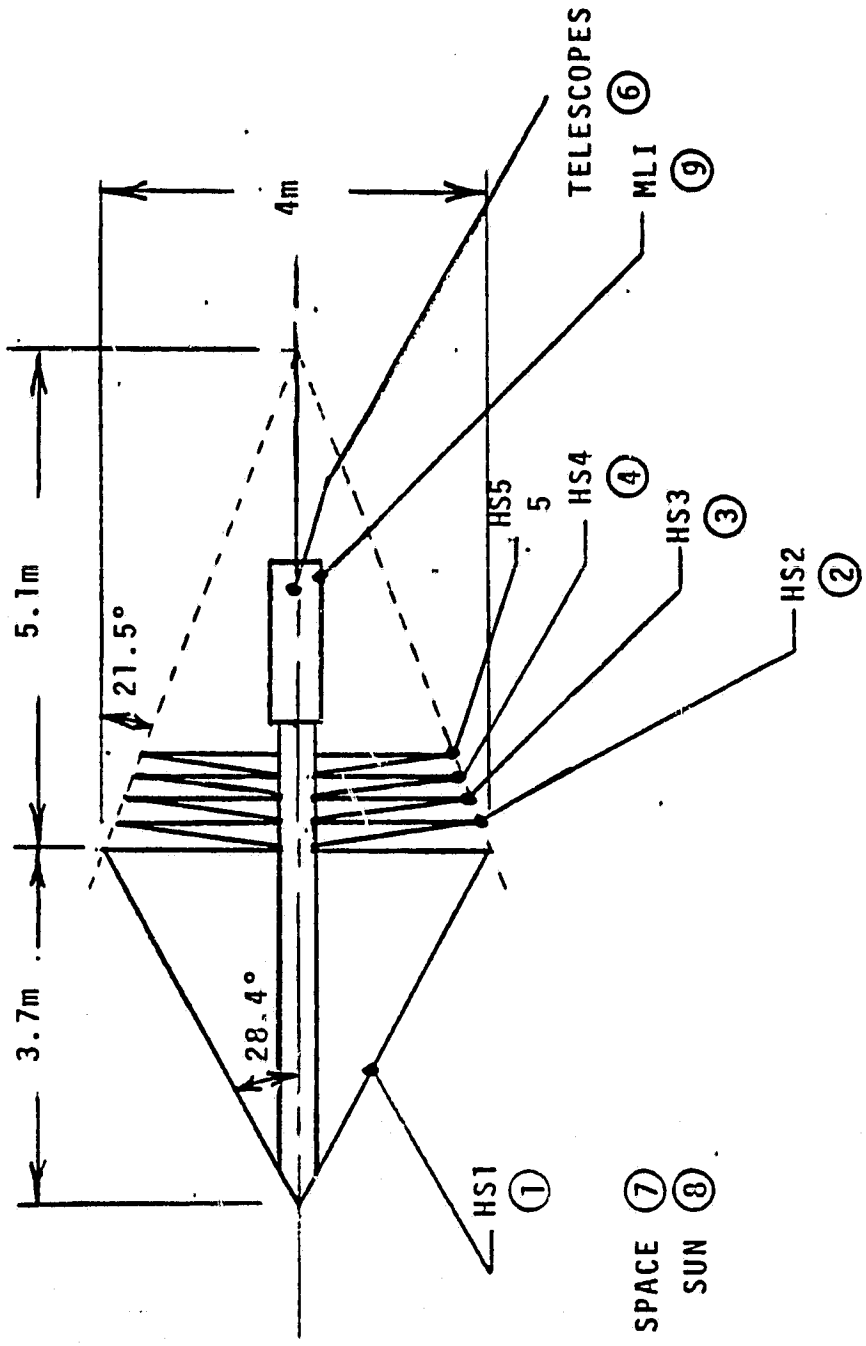

Figure 4-1 Interface Model Thermal Analysis Nodes

TABLE 4-1
THERMAL PROPERTIES

Tungsten (HS1)	$\alpha_s = 0.4$ $\varepsilon = 0.4$
HS1 Open Base	$\varepsilon^* = 0.8$
Tantalum (HS2, 3, 4, 5 and MLI Cover)	$\varepsilon = 0.23$
MLI	$\varepsilon^* = 0.015$
Radiators	$\varepsilon = 0.9$
VUT Interior Structure	$\varepsilon = 1.$
Mirrors	
Optical Surfaces	$\alpha_s = 0.1$
Radiating Surfaces	$\varepsilon = 0.8$
Baffle Tube	$\varepsilon = 1.$

TABLE 4-2
THERMAL EFFECTS OF THE NUMBER OF HEATSHIELDS

NODE	NAME	TEMPERATURE (K)		
		3 SHIELDS	4 SHIELDS	5 SHIELDS
1	HS1	2305	2306	2306
2	HS2	1923	1932	1933
3	HS3	1384	1464	1472
4	HS4	OUT	1053	1116
5	HS5	OUT	OUT	803
6	INSTRUMENTS	467	447	435
7	SPACE	0	0	0
8	SUN	6033	6033	6033
9	MLI	660	504	388

62

TABLE 4-3

TRADE-OFF CONCLUSIONS OBTAINED FROM INTERFACE STUDY

CONCEPT	EFFECT	COMMENT	CONCLUSION
Increase number of heat shields.	Reduces heat load on aperture and exterior of instrument package.	The more the better.	Use the maximum of 5.
Blacken the aft face of intermediate heat shields.	Increase coupling to space, but has minor effect on instrument temperature.	May create an increase in contamination.	Not recommended.
Blacken last shield.	Instrument is hotter.	Last shield is cooler but couples stronger to instrument.	Not recommended.
Lengthen HS1.	Everything is cooler.	Must be deployable to fit envelope-complex.	Not recommended.
Cover base of HS1 with low ε wall.	Heat shields and instrument are hotter.	Increases aperture heating.	Not recommended.
Move instrument to rear.	Instrument is cooler.	Reduces IR heat from baffle into aperture and view of last shield.	Locate instruments as far back as feasible.

A very significant improvement in thermal control was achieved by adding moveable louvers on two side walls near the front of the VUT. The effect of these louvers on the XRT was included in the model. The blockage on the XRT side of the VUT was, therefore, taken into account. In addition, a louver is located on the aft radiator to be closed during the time when the spacecraft is far from the sun and the instrument is off. With all louvers closed and no solar heating, the VUT instrument can be maintained above -40°C (233K) with only about 5W of heater power.

Computer runs were made at 4 solar radii and at 10 solar radii and with the louvers "open" and "closed" in each case. Also, data were obtained with the electrical power "on" and "off" at 10 solar radii. The VUT was assumed to dissipate 5W in its electronics, and the XRT was assumed to dissipate 2.3W of electrical power. The results of the computer runs are given in Table 4-4 and discussed below.

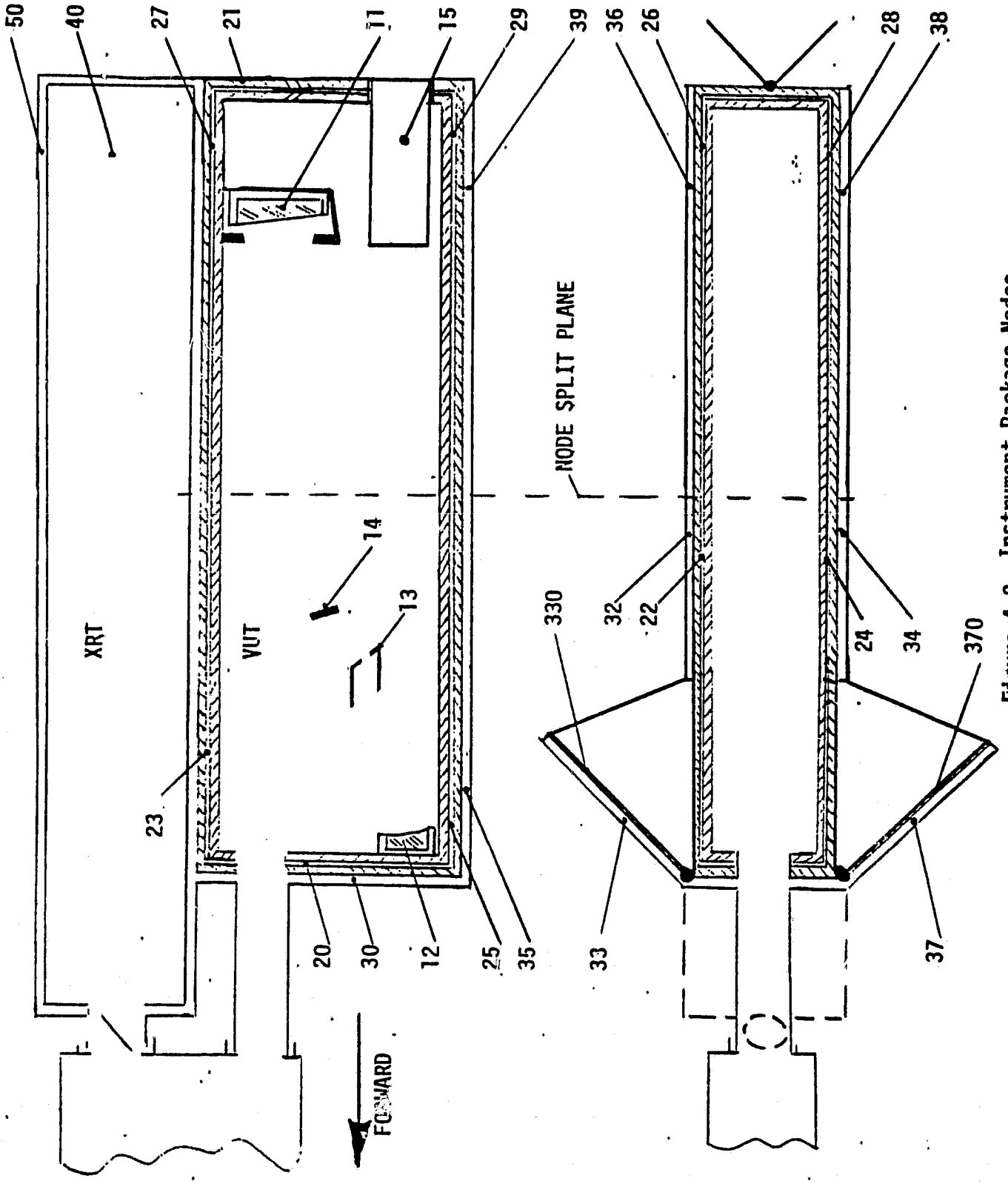

Figure 4-2 Instrument Package Nodes

TABLE 4-4

RESULTS SUMMARY FROM THERMAL ANALYSIS
(AFT LOUVER OPEN)

ORBIT POSITION LOUVER POSITION	4 SOL. RAD. CLOSED	4 SOL. RAD. OPEN	10 SOL. RAD. CLOSED	10 SOL. RAD. OPEN	10 SOL. RAD. CLOSED	10 SOL. RAD. OPEN
POWER (W)						
VUT ELECTRICAL	5.0	5.0	5.0	5.0	0	0
XRT ELECTRICAL	2.3	2.3	2.3	2.3	0	0
VUT APERTURE, SUN/IR NET	25/52	25/54	25/8	25/9	25/8	25/9
XRT APERTURE, SUN/IR NET	22/54	22/54	22/9	22/9	22/9	22/9
TEMPERATURE (K)						
1 HS1	2306	2306	1465	1465	1465	1465
2 HS2	1933	1933	1228	1228	1228	1228
3 HS3	1473	1473	936	936	936	936
4 HS4	1116	1116	709	709	709	709
5 HS5	803	803	510	510	510	510
7 SPACE	0	0	0	0	0	0
8 SUN	6033	6033	6033	6033	6033	6033
VUT NODES:						
11 PRIMARY MIRROR	363	289	303	261	296	256
12 SECONDARY MIRROR	410	298	319	234	312	230
13 FIELD STOP	433	349	365	320	361	318
14 HEAT-REJECT. MIRRORS	449	378	391	356	387	365
15 DETECTOR	369	287	302	254	286	231
20 FRONT WALL	410	297	315	225	308	220
21 REAR WALL	321	244	259	210	251	202

TABLE 4-4 (Continued)

ORBIT POSITION LOUVER POSITION	4 SOL. RAD. CLOSED	4 SOL. RAD. OPEN	10 SOL. RAD. CLOSED	10 SOL. RAD. OPEN	10 SOL. RAD. CLOSED	10 SOL. RAD. OPEN
22 FOR. SIDE WALL	406	276	314	214	307	209
23 FOR. SIDE WALL	407	295	315	228	308	224
24 FOR. SIDE WALL	406	276	314	214	307	209
25 FOR. SIDE WALL	407	296	314	228	308	223
26 AFT. SIDE WALL	374	278	297	231	288	221
27 AFT. SIDE WALL	379	280	301	233	292	224
28 AFT. SIDE WALL	374	279	297	232	288	222
29 AFT. SIDE WALL	381	281	302	233	292	222
30 FRONT MLI	602	600	384	382	384	382
32 FOR. SIDE MLI	299	287	201	185	199	185
33 LOUVER MLI	---	325	---	207	---	207
34 FOR. SIDE MLI	299	287	201	185	199	185
35 FOR. SIDE MLI	299	288	201	186	199	186
36 AFT. SIDE MLI	295	287	197	187	195	186
37 LOUVER MLI	---	325	---	207	---	207
38 AFT. SIDE MLI	295	287	197	187	195	186
39 AFT. SIDE MLI	296	287	198	187	196	186
330 LOUVER	---	250	---	184	---	180
370 LOUVER	---	250	---	184	---	180
XRT NODES:						
40 XRT INST. & RAD. TEMP	280	277	219	217	215	213
50 XRT MLI TEMP.	382	382	244	244	244	244

4.4 BASELINE THERMAL CONTROL DESIGN AND PERFORMANCE

The results of the computer runs of the TAM of the instrument package and spacecraft are in Table 4-4. It can be seen that at 4 solar radii with the front louvers closed, the front of the VUT is considerably hotter than the rear. This is because the heatshield radiation entering the aperture is absorbed primarily by the instrument nodes near the front. These nodes are weakly coupled to the aft surface which is the only area that radiates directly to space. For this reason, louvers were added on two opposite sides near the front as shown in Figure 4-2. The louvers, when open, shade the radiation area from the last heatshield and substitute a reflected view to space. This reduces the gradient in the VUT structure and lowers the average temperature.

At 10 solar radii, a similar effect is observed. With the electronics "on", the structure is warmer than desired with the louvers closed and colder than desired when the louvers are open. An intermediate position will produce the desired temperatures. Similarly, when the electronics is "off" the desired temperatures will result with the louvers partially open; somewhat less open than when the electronics are "on".

The conclusion is that each louver should be positioned by a proportional controller that senses the structure temperature under it. In this way the temperatures can be controlled to ±10K in level and gradient, well within the margins, assumed in Section 3.2.2.

The magnetometer, detector and associated electronics are located in a common package that is mounted to the optical bench with conductively isolating supports. The package has a separate radiator to space out the aft wall of the VUT. The package has 5W of electrical power and absorbs 4.4W of solar power. The package can be maintained cooler than 20°C with the louvers open. The detector temperature can be set by correctly choosing the relative area of the aft radiator that is directly attached to the detector package.

The louver for the aft wall radiator gives added thermal control during the observations and also reduces the heater power required to maintain the

instrument above its minimum storage temperature prior to encounter with the sun. A computer run with no sun and the aft louver closed calculated only about 5W was required.

We have also investigated the desirability of a moveable shutter over the VUT aperture to block radiation from the baffle and direct sunlight. The shutter could be in the form of a 45-degree specular mirror that reflects the incident energy away to space. The relatively collimated sunlight will be reflected in a narrow cone. However, the diffuse radiation from the baffle will be reflected in a diffuse pattern, and it will be difficult to keep it off of other components behind the last heatshield. A mirror that is orientated normal to the baffle axis will reflect the energy back into the baffle, and this may be the better choice. In either case, the shutter will be elevated in temperature close to that of the last heatshield and will reradiate into the instrument. The closed shutter will reduce the aperture heat load by a factor of 8 if the emissivity of both sides of the shutter $\varepsilon = 0.25$. Likewise, the heat loss from the instrument out the aperture when the spacecraft is far from the sun will be reduced by a factor of 8 when the shutter is closed. This reduces the heater power required to maintain the instrument above the minimum storage temperature, but this is not significant since the power is only 5W. It is certainly true that a shutter at the instrument is in a better thermal environment than if it is "out front". However, it may still be too hot to work reliably during the encounter by cycling between exposures. At 4 solar radii, the primary mirror and electronics change about 0.7K for each watt applied to the instrument through the aperture. For a reduction of 70W, the components will run about 50K cooler.

The operational sequence for the VUT thermal control is shown in Table 4-5. If the louver thermostats are set to maintain forward-side-wall temperatures of 300K (modes 22 and 24), the temperature of the primary mirror varies from 297K at 10 solar radii to 303K at 4 solar radii, as follows by interpolation from Table 4. The corresponding secondary-mirror temperatures are 307K and 318K, respectively. This is the basis for the mirror temperatures, assumed throughout this report.

Table 4-5
THERMAL CONTROL SEQUENCE

Phase	Louver Position	Heater	Electronics
Launch/Earth Orbit	Closed	Off	Off
Earth/Jupiter/Sun Transits	Closed	On	Off
Sun Approach	Gradually Opening	Off	Off
10 Solar Radii	Partially Open	Off	On
4 Solar Radii	Full Open	Off	On
10 Solar Radii	Partly Open	Off	On
Post Encounter	Closed	On	Off

4.5 CONCLUSIONS AND RECOMMENDATIONS

- A feasible thermal control concept for the VUT is identified. It controls the VUT temperatures within acceptable limits throughout the mission. The use of low-expansion optical mirrors and graphite/epoxy optical bench permits operation within ±20K which is wider than the expected ±10K control expected by the thermal control concept.

- The use of thermostatic active louvers reduces the uncertainty in temperature control that exists in a purely passive design.

- The thermal design is not final, since a greatly simplified spacecraft interface was assumed. However, the concept has margin in radiator size and louver configuration that will accomodate changes in instrument configuration. The XRT would seem to require a similar thermal design.

69

- The thermal analysis model (TAM) developed during the study, has enough detail to be useful in tracking the evolutions in the Starprobe project. Additional detail can be added, if needed, to examine evolutions in the system during future studies.

- Five heatshields (the primary and four secondary) are the maximum that will fit the envelope and all should be used.

- Items that require further study include:
  (a) Thermal distortion of primary and secondary mirror from -10 hrs to +10 hrs from perihelion (Section 3.2.2.4).
  (b) Additional detail of the mechanical design of the graphite epoxy optical bench and support system that minimizes thermal distortion from the mounts.
  (c) More detailed definition of the number of metal foil layers and aluminized Kapton layers required for the MLI blankets, along with design of blanket support and spacer system.
  (d) Detailed analysis of louver configurations with respect to heating of the inside of the radiators by direct radiation from HS5 and radiation, reflected off the instrument MLI.
  (e) Selection of control mechanisms for louver positioning.
  (f) Better definition of the electronics power within the telescope, compared to location of some in a remote box on the spacecraft platform.
  (g) Feasibility of shutter operation between exposures at 10 sun radii when the motor may be near 200°C (473K), or when operation is needed during storage.

Section 5
IMPLEMENTATION

This section summarizes some preliminary ideas on implementations. All of these should be subject to further feasibility studies.

5.1 STRUCTURE AND MOUNTING

The optical components must be mounted on an athermal optical bench. Two approaches suggest themselves:

- o graphite-epoxy tubular truss,
- o ULE or Cervit metering structure.

The optical bench must be enclosed in a protective housing. We assume here a ribbed aluminum box, in which the optical bench is kinematically supported. The housing is protected by multilayer insolation (MLI) against direct radiative heating, except where temperature-control louvers are installed.

To mount the VUT in the spacecraft, two mounting rings, separated by an A-frame structure, as indicated in Figure 1-1, could possibly be provided. By mounting the VUT and the XRT as a single unit, best coalignment between the two imaging instruments is assured.

Graphite-epoxy optical bench. An open truss has the advantage over a monocoque structure that the instrument can come to rapid thermal equilibrium by radiative coupling of the housing walls. Another advantage is that the truss can be built up of separate tubes, which can be individually tested for their thermal expansion properties.

One problem that might arise with the use of graphite-epoxy in the VUT would be the release of contaminants during the long voyage to the sun. These might form a deposit on the mirrors and subsequently be polymerized by UV solar

71

radiation. Although graphite-epoxies exist with an extremely low rate of emanation, the question remains whether near-zero thermal expansion near 300K can be realized at the same time. This would require further detailed study.

A second problem might be dimensional variation with moisture content. In principle, it would be possible to focus and align the VUT while the structure was completely dry. Subsequent absorption of water vapor might introduce dimensional changes, but complete restoration should occur when the moisture is desorbed during flight. This, too, requires further study.

ULE or Cervit metering structure. The simplest approach would be to support the primary and secondary mirrors laterally from the housing and use ultra-low-expansion rods as spacers between the mirror cells. This would eliminate the largest contribution to the isothermal focus change (Table 3-4). An alternate solution would be to connect the mirror cells by an A-frame structure. This provides lateral stability as well. If this approach is taken, suitable materials for the mirror cells and the interfaces with the metering structure also have to be identified.

5.2 MASS AND SIZES

Mass and size estimates, based on the optical parameters of Table 3-9, are summarized in Table 5-1. An overview of the structural concept is shown in Figure 1-2. Unfortunately, the mass estimate exceeds the allowances, made in Ref. 1 (13kg) for the visible-light/UV imaging instrument. For these estimates, engineer principles, applicable to earth-orbit instruments, were assumed. Perhaps some mass reduction is possible by more rigorous adherence to deep-space probe engineering practice.

5.3 MIRRORS AND COATINGS

Solid mirror blanks would seem to be least susceptible to thermal deformation, if irradiated uniformly. In first-order approximation, the deformation is independent of thickness. It is, perhaps, possible to apply blanks with a

72

Table 5-1
MASS, SIZE AND POWER ESTIMATES

MASS (kg)	
Optical bench	4.5
Housing	11
Mounting structures	2
Louvers	2
Contingency	1.8
Thermal insulation	0.8
Mirrors and cells	1.1
Stops and baffles	0.7
Heat-rejection mirrors	0.6
Scientific instrument	1
Electronics/cables	2.5
Total	28.0
SIZE (cm)	
Optical bench	97 x 32 x 17
Housing (outside)	105 x 40 x 25
POWER (W)	
Detector and internal electronics	5

13

higher diameter/thickness ratio than 6 or 8, the standard ratio for larger telescope mirrors. Whether light-weight blanks would be acceptable might also be investigated.

There is no a priori reasons why an Al/MgF_2 mirror coating could not withstand irradiation by 6.5 suns (as predicted for the primary mirror), if the substrate can be held to a temperature of 300K (27°C). However, further study is required. Experience with mirrors for high-power laser optics would provide valuable information. Alternate coatings might also be evaluated.

5.4 HEAT-REJECTION SYSTEM AND SHUTTER

Both the heat-shield tube and the VUT housing must be provided with internal baffles to suppress reflections from the inner surfaces. Whether these should be absorptive or reflective has not been addressed in this study. The baffle, immediately in front of the primary mirror, should match the thermal properties of the latter, and definitely be built as a heat-rejection mirror. A spherical surface, with the center of curvature in the instrument aperture, would reflect all incident radiation back through this aperture.

Another heat-rejection mirror must be placed at the prime focus. A solid flat metal mirror, with a perforation to act as the prime-focus fieldstop, would seem suitable. A second, concave mirror focuses the rejected radiation on the center of the instrument aperture. Both mirrors must be heat-sunk to the instrument housing. A diagram of the prime-focus area is shown in Figure 5-1. It shows that the entrance-pupil decentering distance, assumed in Section 3.3.2 (b = 135mm) indeed allows all structural elements in this area to be fitted in, with sufficient margins to assure clearance of the optical beams.

As pointed out in Section 4, a shutter would help significantly in the reduction of the heatload of the instrument. However, if control by louvers only is found to be adequate, the added complexity of a shutter would not seem warranted. In principle, the shutter could be driven by a motor with gear train within the instrument, to which it is connected by a highly insulating shaft (e.g.

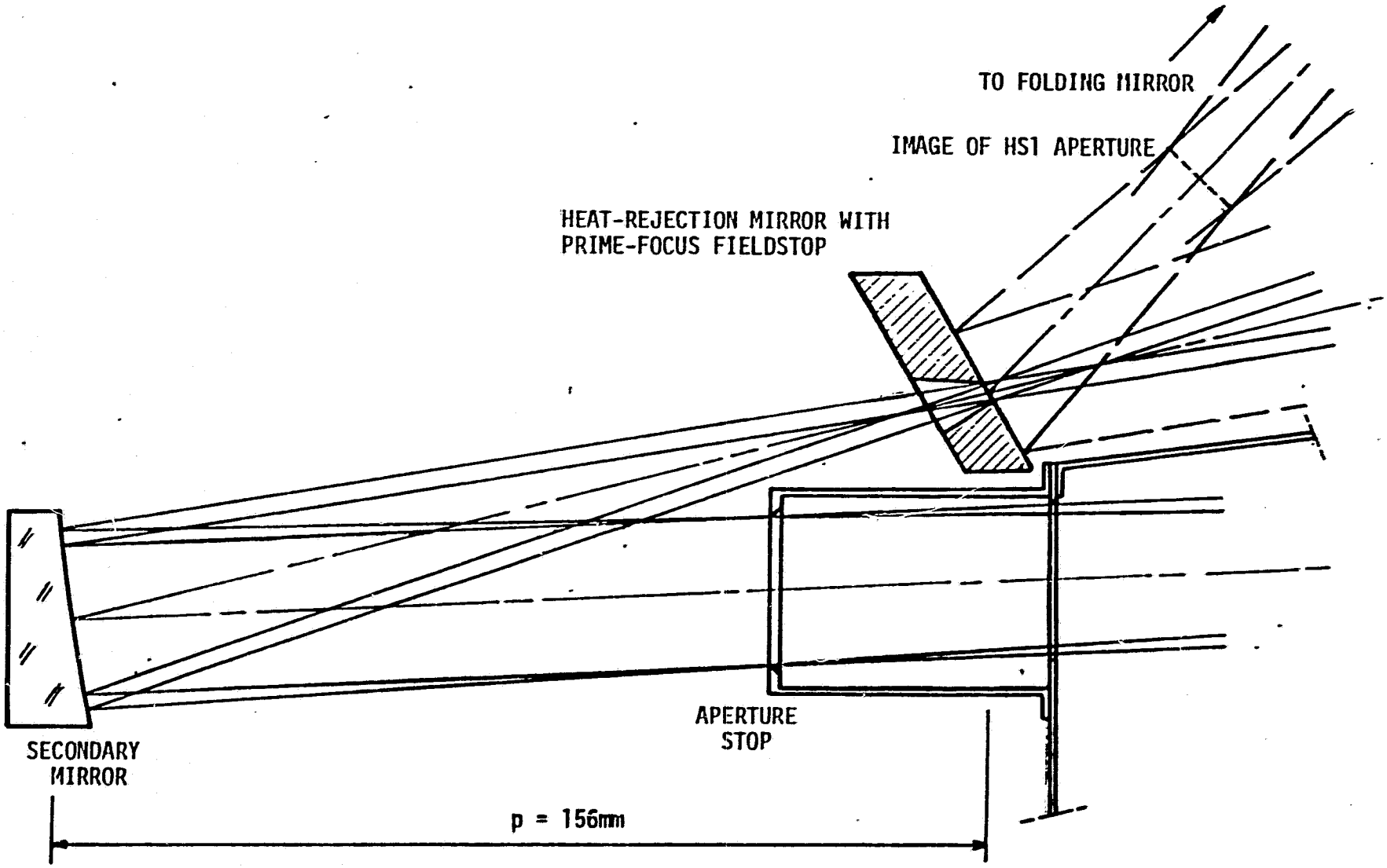

Figure 5-1 Prime-focus area with heat rejection mirror and aperture stop. The heat-rejection mirror reflects the full image, formed by the primary mirror of the HS1 aperture to the folding mirror (not shown).

thin-walled stainless steel tube). The implementation is not further investigated here. We note that opening and closing of the shutter would cause a fluctuation in temperature. This does not occur with louvers.

5.5 SCIENTIFIC INSTRUMENT ACCOMODATION

The preliminary VUT concept leaves ample room for scientific instruments. One candidate instrument would be a magnetometer of the type, described by Title (Ref. 12). According to information, received from Title, the diameter would be about 5cm and the length about 10cm (Ref. 13). The mass would not exceed 1kg. A report, describing this instrument in detail, is in preparation, but was not available for this study.

Multiple scientific instruments might be considered if the Starprobe mass budget permits. Dichroic mirrors might be used to separate visible light from the UV. Alternatively, the telescope beam could be directed consecutively to different instruments by means of a mirror carousel. None of these options have been addressed in this study.

5.6 IMAGE-MOTION COMPENSATION

In order to prevent significant MTF losses, the image must be stabilized during each exposure to about 0.2 of a resolution element. Residual image displacements with a rms amplitude σ cause a reduction in MTF, equal to

$$R_i(\nu) = \exp(-2\pi^2\nu^2\sigma^2), \qquad (1)$$

where ν is the spatial frequency. If we require, for instance, $R_i(\nu) \geq 0.8$ at $\nu = 33.3$ cycles/mm, we find $\sigma \leq 3.2\mu m$. The angular resolution, corresponding to this frequency is $10\mu rad \approx 2$ arc sec. The telescope/detector MTF at $\nu = 33.3$ cycles/mm is $R(\nu) \approx 0.14$ (Section 3.1). Residual image motion with $\sigma = 3.2\mu m$ then reduces the system MTF to

$$R_i(\nu)R(\nu) \approx 0.11.$$

According to Title, a quadrant silicon photodetector could be used as a position sensor (Ref. 13). Motion of the image of a granule near its center produces differential signals in two orthogonal directions, that can be used for bi-axial control of an element in the optical train. The sensing accuracy is limited by photon statistics. This defines the minimum sampling time τ that is required. The spacecraft pointing rates should not be much larger than σ/τ, in order to assure stable motion compensation. The sensor must be placed as close to the image plane as possible. A small folding mirror outside the CCD area but within the 17mm diameter field would be best.

In the VUT, the only optical element, available for articulation, is the secondary mirror. Tilt of this mirror around its vertex will cause coma in all field points (Section 3.2.2). This can be eliminated by tilting the mirror around its so called "neutral point" (Ref. 14). In the VUT, this point lies at a distance of 152mm from the secondary mirror, close to the prime focus. Articulation around the neutral point complicates the actuator mechanisms. Whether articulation around the vertex would be acceptable, depends on the magnitude of the spacecraft pointing errors. Obviously, the IMC system can only be developed in close conjunction with the spacecraft pointing and stabilization system. This would certainly merit a separate feasibility study.

5.7 CONCLUSIONS

- A preliminary estimate indicates larger mass and size than allotted for in earlier Starprobe studies (Ref. 1).
- Additional study is needed in the following areas:
  - Long-term stability, moisture control and outgassing of graphite-epoxy, especially with regard to UV polymerization of condensation products.
  - Implementation of alternate Cervit or ULE metering structures.
  - Stability and reflectance of Al/MgF_2 coated mirrors in the Starprobe environment.

77

- A technical feasibility study is recommended on implementation of image-motion compensation in relation to spacecraft pointing accuracy and pointing rates.

78

Section 6
GENERAL CONCLUSIONS AND RECOMMENDATIONS

The principal purpose of this study was to evaluate whether imaging in visible light/UV from Starprobe was feasible at all. At the end of the study, no compelling reason was found why this should not be the case. This conclusion is based on the following approach to the design of the imaging instruments:

a. The visible-light/UV telescope (VUT) and the X-ray telescope (XRT) have separate light paths through the central baffle tube, rather than a common path as in earlier concepts. This has two advantages:

   - o Relay optics to extract the VUT beam from the XRT beam are eliminated.

   - o The VUT does not impose a lower limit on the XRT aperture diameter. Indeed, the XRT concept, developed by American Science and Engineering in a separate study, would not be compatible with the VUT if a common light path was maintained.

b. The VUT is conceived as an off-axis, aplanatic gregorian telescope. This has the following advantages:

   - o Best image quality with minimum collecting area.

   - o Uniformly irradiated primary mirror with least susceptibility to thermal deformation.

   - o Accessible field and aperture stops for effective heat rejection and straylight suppression.

   - o Adequate focus and alignment stability, provided mirror and structure materials with sufficiently low expansion at the operating temperatures can be found or developed.

79

c. Thermal shielding by a total of five heatshields (primary and four secondary heatshields), combined with a radiator and two additional thermostatic louvers keeps the instrument temperature constant at about 300K (27°C) from -10 hours to +10 hours from perihelion passage. This offers highly stable conditions for continuous observations.

In the course of the study, the following problems were identified:

- The irradiation of the primary mirror is still high (6.4 suns, not counting the reradiation from the heatshields).
- The effect of this irradiation on the mirror coatings remains unknown.
- The overall mass of the instrument (28kg) exceeds the allottment, made in earlier studies (13kg).

On the basis of these findings, the following items are recommended for further study:

- Analysis of thermal deformations of the telescope mirrors and resulting effects on image quality in greater depth than was possible in the present study.
- Experimental investigation of mirror deformations at 6.4 suns. This could also include a comparative study of mirror coatings.
- Study of additional means for lowering the instrument temperature, e.g. by a controllable shutter. Some means to close the instrument during the voyage to the sun will probably be needed anyway.
- Investigation of thermal properties and dimensional stability (including sensitivity to moisture) of graphite epoxies in view of the rapid technological development of these materials.

- Detailed study of contamination control techniques and screening of candidate materials with respect to UV photopolymerisation.

- Search for means to reduce the overall instrument mass by use of lighter structures, light-weight mirrors and/or more compact optical train.

Additional conclusions and recommendations are listed at the ends of Sections 2, 3, 4 and 5.

REFERENCES

1. "Starprobe Science Options Review", JPL 725-42, 6 January 1981

2. "Starprobe, an Interim Report", American Science and Engineering Inc., Arlington, MA, Report ASE-4652, 2 July 1981

3. "Solar Probe Advanced Development", JPL 715-44, 1 June 1980

4. JPL private communication, 10 July 1981

5. "Solar Probe Optics Study", JPL Vellum 79-32, 1979

6. C.W. Allen, "Astrophysical Quanties", Athlone Press, 1964, Chapter 9

7. H.S. Hudson in "A Close-Up of the Sun", JPL 78-70, September 1, 1978, page 81

8. H. Zirin, Reference 7, page 89

9. M. Bottema and R.A. Woodruff, Applied Optics 10, 300 (1971)

10. "SOT/Starlab Compatibility Design Study", BASD, Final Report F79-11, November 1979, Section 3.5

11. CIT Photoheliograph Definition Study, BBRC Final Report F71-02, April 1971

12. A.M. Title, Reference 7, page 155

13. A.M. Title, Lockheed Palo Alto Research Laboratory, Palo Alto, CA, private communication

14. W. Wetherell and M.P. Rimmer, Applied Optics 11 2817 (1972)

APPENDIX A

A DESIGN STUDY OF IMAGING TECHNIQUES FOR THE STARPROBE MISSION

INFORMAL STUDYPLAN

M. Bottema

Contract 955929 between
California Institute of Technology
Jet Propulsion Laboratory
4800 Oak Grove Drive
Pasadena, California 91103

and

Ball Corporation
Ball Aerospace Systems Division
P.O. Box 1062
Boulder, Colorado 80306

May 1, 1981

A DESIGN STUDY OF IMAGING TECHNIQUES FOR THE STARPROBE MISSION

INFORMAL STUDYPLAN

The purpose of the study is to evaluate the technical feasibility of imaging techniques that can be used for the Starprobe mission, and to compare the applicability of various instrument concepts. Accordingly, we plan the following study approach:

1. Compare various candidate instrument configurations for the three imaging experiments, specified in the SOW, i.e. a magnetograph/doppler velocity detector, an X-ray telescope and an XUV telescope.

2. Compare various candidate instrument concepts for the above three experiments in terms of their compatibility with Starprobe. Specific areas that will be addressed are discussed in detail below:

1. <u>Candidate configurations</u>

   A number of candidate configurations was compiled in preparation of this study plan. This overview is attached as appendix A, We plan to address primarily the following options (lettered as in Figure 2.1):

   a.1 Configuration described in "Starprobe Science Options Review," JPL 725-42, 6 January, 1981.
   a.2 Modification of above with crossed folding mirrors for polarization compensation (not shown in Figure 2.1).
   e. Coaligned X-ray and visible-UV telescopes without fore optics, sharing a large aperture in the heat shields.
   j. Non-aligned X-ray and visible-UV telescopes without fore optics, sharing small aperture in primary heatshield.

We plan to treat the remaining configurations with lower priority, unless directed otherwise by JPL.

84

The specific areas of study will include:

- o Heat inputs to scientific instruments and deflection optics.
- o Thermal deformations of deflection optics and mounting structures and its effects on alignment.
- o Improvement of thermal environment by additional heat-shields and/or enclosures.
- o Effects of variation in thermal environment from -10 hours to +10 hours from encounter.
- o Control of insolation by means of a shutter.
- o Materials, coatings and polarization properties of deflection optics.
- o Contamination control.

2. Scientific instrument concepts

2.1 Visible-UV telescope

The prime candidate for the visible-UV telescope is either a centered or an off-axis gregorian telescope. A preliminary concept has been developed which shows good image quality in the required field (a detailed report is in preparation). This "strawman" concept will be used to evaluate the following:

- o Sensitivity to thermal deformations.
- o Thermal control concepts and heat rejection from -10 hours to +10 hours from encounter.
- o Mirror materials and coatings.
- o Straylight suppression and radiation shielding.
- o Thermal control of detectors, operating and non-operating.
- o Packaging and mounting.

Other telescope concepts will be studied if so directed by JPL.

85

2.2 X-ray telescope

We consider a single Wolter-II type telescope as the prime candidate. A preliminary "strawman" design has been completed (a report is in preparation). The same engineering aspect will be studied as listed in Section 2.1. Special attention will be given to the highly critical tolerance sensitivity and also to the relation between physical telescope length and collecting area.

Other candidate concepts are:

- o pinhole cameras,
- o coded-aperture cameras (including zone plates),
- o Kirkpatrick-Baez telescopes.

These concepts differ greatly in scientific applicability. We plan to review the main engineering aspects of these concepts in comparison to the Wolter-II type telescope.

3. Analysis methods and information required

In compliance with the SOW, we present here a brief overview of the analytical methods that will be used and the information that will be required from JPL.

3.1 Optical design

Concepts are developed "by hand" to the third-order level and subsequently refined by means of the ACCOS-V exact raytracing program. This will allow evaluation of image quality in terms of geometrical aberrations, as well as diffraction point-spread functions and MTF's. The program also permits tolerance analysis and the modeling of deformed mirror surfaces.

3.2 Thermal and structural analysis

A variety of programs are available at BASD. These will amply suffice to perform the tasks needed for this study.

86

3.3 Information required from JPL

Most valuable will be recurrent updates on the thermal loads of the deflection optics and the external loads of the scientific instruments. Specific data will be requested as the study proceeds.

3.4 Material properties of imaging-system components

The main source of information will be vendor catalogs and contacts. Previous analysis, performed at BASD on several solar instruments, will also be available.